

# Seasonal Characteristics of the Perennial Ice Cover of the Beaufort Sea

R. Kwok, J. C. Comiso\* and G. F. Cunningham

*Jet Propulsion Laboratory  
California Institute of Technology  
4800 Oak Grove Drive  
Pasadena, CA 91109*

*\*Laboratory for Hydrospheric Processes  
Goddard Space Flight Center  
Greenbelt, MD 20771*

Submitted to *JGR - Ocean*

January 23, 1996

Please send correspondences to:

Ronald Kwok  
Jet Propulsion Laboratory  
California Institute of Technology  
MS 300-235  
4800 Oak Grove Drive  
Pasadena, CA 91109

# Seasonal Characteristics of the Perennial Ice Cover of the Beaufort Sea

R. Kwok, J. C. Comiso and G. F. Cunningham

## Abstract

By definition, ice which survives the summer is classified as multiyear ice. Thus, the area covered by multiyear ice during the winter should be nearly equivalent to the ice area during the previous summer's minima. This condition provides a reasonable criterion for the evaluation of ice concentration and ice type retrieval algorithms using remote sensing datasets. From SSMI data, the NASA Team algorithm estimates the multiyear, first-year and total ice concentrations during the winter using combinations of the polarization and spectral gradient ratios. The Team algorithm provides only estimates of ice concentration in the summer. From ERS-1 SAR data, the remarkably stable contrast between multiyear ice and first-year ice provides consistent estimates of multiyear ice concentrations. In the summer, multiyear ice concentration cannot be estimated from SAR or SSMI data because free water on the surface effectively masks the backscatter and emissivity signature of this ice type. From SAR data, a technique which takes advantage of the high backscatter of wind-roughened open water as a discrimination feature is used to estimate the total ice concentration in the summer. With a year long (Jan 92 to Jan 93) dataset from the Beaufort Sea, we found that the multiyear ice concentration estimates from the SAR data to be very stable and *are* is nearly equivalent to the ice concentration estimated at the end of the previous summer. We contrast this with the variability of the MY ice concentration and ice fraction estimates obtained using SSMI data. The Team algorithm produces ice concentration and multiyear ice estimates which are consistently lower than those from the SAR data. We suggest reasons for these discrepancies and discuss the implications of the higher than previously noted multiyear ice concentrations on mass balance studies.

# 1 Introduction

The total ice and multiyear ice concentrations estimated using the NASA sea ice algorithm [Cavalieri *et al.*, 1985-1] or Team algorithm provide a fairly long temporal record of the character of the polar ice cover using data from the Scanning Multichannel Microwave Radiometer (SMMR) and its successor, the Special Sensor Microwave Imager (SSM/I). If the seasonal records are examined, one finds that the retrieval algorithm provides estimates of multiyear ice concentration in the winter which are much lower (by up to 30%) than that of the summer ice concentration. From an ice balance perspective, such large discrepancies need to be resolved. If ice which survives the summer is classified as multiyear ice, then the multiyear ice concentration during the winter should be nearly equivalent to the ice concentration during the previous summer's minima, differing by an amount due to melt, ridging, new/young ice formation and export of ice from the Arctic. This mismatch was noted by a number of investigators from the point of view of variability of the multichannel microwave signatures of sea ice from SSM/I in regional studies [Thomas, 1993] and surface measurements [Grenfell and Lohanick, 1985; Grenfell, 1992], and from an ice balance point of view [Comiso, 1990; Rothrock and Thomas, 1991; Rothrock and THOMAS, 1993].

Currently, the Team algorithm provides the only long-term record of multiyear ice and total ice concentration derived from objective analysis of the passive microwave observations. The only other estimate we are aware of was made by Wittmann and Schule [1966] which gives a multiyear ice concentration of over 70%, is based on aerial surveys. It is apparent that better multiyear ice observations are needed to establish the true nature of the ice cover. Validation studies for the Team algorithm shows overestimates in some areas and underestimates in others [Cavalieri *et al.*, 1992]. Rothrock and Thomas [1991] used a Kalman filter/smoothing to couple a physical model and the Team algorithm analyses to obtain optimal estimates of the total ice and multiyear ice concentrations to overcome some of the difficulties of the raw observations and to provide a more consistent temporal record of the ice cover. The Kalman filter increases the winter multiyear ice concentration and decreases the summer ice

concentration so as to eliminate the inconsistency between the summer and winter concentration estimates from the Team algorithm. As they noted, the filtered estimates would be biased if the measurements are themselves biased. They demonstrated that the assumption of pure signatures introduces biases in the Team algorithm estimates.

With the launch of the European Earth Remote Sensing Satellite (ERS-1) in July of 1991, this C-band Synthetic Aperture Radar (SAR) has provided a different view of the ice cover than that offered by the SSMI sensor. The much higher resolution allows us to distinguish between floes and leads most of the time, and there is sufficient backscatter contrast between ice types that their identification is possible under certain conditions (discussed more later). The limitations of sensor swath width (1001 ml), orbit orientation and lack of an onboard tape recorder, however, did not provide a system suitable for routine monitoring of the Arctic sea ice cover in the SSMI fashion. However, comparison of the seasonal record of regional ice concentrations estimated at coincident SAR and SSMI locations are possible and offer another independent characterization of the state of the sea ice cover. Here, we compare the ice concentrations derived from a set of SAR data and the same ice concentrations estimated using the Team algorithm. The questions we would like to ask are: (a) how do the average total and multiyear ice concentrations vary over a seasonal cycle; and, (b) how accurate are the estimates from passive microwave data? A comparative study of results from SSMI and SAR data is made here to gain insight into some answers to these questions.

As a basis for evaluation of the retrieval algorithms, we would like to present a simplified view of the character of the annual cycle of the Arctic sea ice cover (shown in Fig. 1) based on our definition of multiyear ice. The validity of the estimates of the ice concentration obtained using the Team and SAR algorithms are measured against these trends. In the winter, the areal extent, of multiyear ice remains fairly constant with a small decrease due to ridging and export of ice through the Fram strait. The total ice concentration stays close to unity because water in open leads freezes rapidly at sub-freezing temperatures. The first-year ice concentration increases as the ice in previously open leads thickens and able to survive the mechanical stresses within the ice cover. After the spring/summer transition, the total

ice, multiyear and first-year ice concentrations would start to decrease due to lateral melt because of the above-freezing air temperatures throughout the Arctic. Very little first-year ice is produced during the summer. At the end of the summer, all the ice in the Arctic Ocean becomes multiyear ice (by definition) resulting in a sharp increase in the multiyear ice concentration. Consequently, the multiyear ice concentration at this time should be roughly equivalent to the ice concentration at the summer's end. This cycle is then repeated during the next ice season. We note here that this is more valid as a regional view rather than a large scale view. On the Arctic scale, the seasonal transitions occur at different dates at different locations and the transitions themselves are not as sharp as the view presented here.

In this study, we present results of a comparative analysis of the multiyear ice concentration estimates from the Team algorithm and the SAR retrieval algorithm using a dataset spanning January 1992 through January 1993. We also compare total ice concentrations and discuss the differences in the three periods separated by the onset of melt during the spring/summer transition and the fall freeze-up during the summer/winter transition. The differences are examined in terms of consistency in the analysis and the effect of signature variability on these estimates. The implications of these differences on the multiyear ice balance and computation of the actual ice cover are discussed.

## **2 Data Description**

### *Region of Study*

The region we selected for the comparison is shown in Fig. 2. The shape of the eastern and western boundaries of the region are defined by ERS-1 orbits used in this study. The southern boundary is at approximately  $70^{\circ}\text{N}$  and the northern boundary is at approximately  $85^{\circ}\text{N}$ .

### *SSM/I Data*

Brightness temperatures from all SSM/I channels were gridded to a standard rectangular polar stereographic format for analysis of the dual polarized multispectral data. Daily averages were mapped to a 304 by 448 matrix with a grid size of 25 km by 25 km. Only the 19 and 37GHz channels are used in the retrieval of total and multiyear ice concentrations. The 22GHz channel is also used but only as an ocean mask. The radiometer observations are made at an angle of incidence of  $53.1^\circ$  at the Earth's surface and at a swath width of  $139^\circ$  E-W.

### *SAR Data*

We selected a total of 571 ERS-1 SAR images between January 1992 and January 1993 for the comparative analysis. This represents approximately 44 images per month. All the SAR images for a particular month were collected within a three-day period early in the month. The sensor is a C-band (5.3GHz) radar operated with vertical transmit and receive polarizations at a look angle of  $20^\circ$ . Within the antenna beam, which illuminates a swath of approximately 100km in width, the incidence angles on the ground vary from  $19^\circ$  at near range to almost  $26^\circ$  at far range. The image data used in this study were received and processed at the Alaska SAR Facility (ASF) in Fairbanks, Alaska. Each image frame covers an area of approximately 100km by 1001km. The image data used in this study have a sample spacing of 100m. This lower resolution data type was selected because the lower speckle content reduces the uncertainty in the estimates. Ancillary data are provided with each image frame for calibration and conversion of the 8-bit digital data into normalized backscatter cross-sections.

The SAR analysis algorithms we use requires a calibrated dataset because the identification of the sea ice types is based on tabulated expectations of the backscatter [Kwok et al., 1992]. Calibration of the radar is measured in an absolute and relative sense. The absolute calibration accuracy metric quantifies the uncertainty in the observed normalized backscatter cross-

section ( $\sigma_o$ ) measurement relative to the actual  $\sigma_o$  of a distributed target. Typically, this appears as a bias when an identical target from two image frames (imaged at different times) are compared. The in-scene variance of a radar target known to have uniform backscatter cross-section is measured by the relative calibration accuracy of the data. Relative calibration is usually better than absolute calibration and is easily maintainable especially if the radar sensor is stable. The data products used in this study have expected absolute and relative accuracies of 2dB and 1dB, respectively.

### *Wind and temperature fields*

Surface wind and temperature fields obtained from the from National Meteorological Center (NMC) were gridded at (2.5° latitude by 5° longitude grid) at two daily intervals centered at 00Z and 1200Z. In the NMC analysis process, the observations are interpolated to a grid. Because large parts of the world have no observations and the data are not taken at one time (observations are included if it is within 6 hours of the forecast time), NMC uses a model forecast to help with the interpolation. Therefore, the data provided are a blend of observational and model data. While the temperature fields may not represent the actual physical surface air temperature due to uncertainty in the NMC analyses (typically the temperature fields are biased due to difficulty in modelling the inversion layer), they are nevertheless good indicators of the surface conditions.

## **3 Data Analysis**

We describe the algorithms used in our analysis and their expected precision. The details of these algorithms and their limitations, especially the Team algorithm, have been discussed in the references provided below. Here, we provide a more detailed accounting of the SAR algorithms since they are relatively recent developments. In the remote sensing of the ice types of interest here, we would like the ice layer rather than the surface cover to provide the largest contribution to the observed signature such that the retrieval algorithms are



not confounded by surface effects. These algorithms are dependent on the stability of the signature of ice types for correct interpretation of the active and passive microwave data. The variability of the passive and active sea ice signatures are typically affected by surface conditions. Surface processes typically affect the shorter wavelength observations and lower frequencies are less affected by the atmosphere and minor modifications of the snow layer.

#### *Ice concentration from SSM/I data*

Brightness temperatures from all SSM/I channels were gridded to a standard rectangular polar stereographic format for analysis of the dual polarized multispectral data. Using the spectral gradient ratio (GR) at 37 GHz and 19 GHz, and the polarization ratio (PR) at 19 GHz, the concentration of open water, first-year ice and multiyear ice are computed at each 25 km cell using the NASA Team algorithm [Cavalieri *et al.*, 1984; Gloersen and Cavalieri, 1986]. The procedure to estimate the total ice and ice type concentrations in an SSM/I pixel is based on a mixing formulation which assumes that multiyear ice, first-year ice and open water have temporally and spatially stable signatures. The precision of the open water estimates, in the Beaufort and Chukchi Seas, ranges between  $-2.1 \pm 3.1\%$  and  $0.6 \pm 7.4\%$  [Cavalieri, 1992]. The variance in the multiyear ice estimates, when compared with estimates from other sensors, are higher and trends are not evident. The reader is referred to Cavalieri [1992] for a summary of the uncertainties in the Team algorithm-derived ice concentrations.

#### *Ice type concentration from ERS-1 SAR data in winter*

In the winter, we derive open water, first-year ice and multiyear ice concentrations using an algorithm described in Kwok *et al.* [1992]. The algorithm uses a fairly simple backscatter-based classification scheme to identify the different ice types. Each pixel is classified into one of the three categories. No attempt is made, because of the higher resolution of the SAR data, to resolve the different types within a pixel as is done in Team algorithm. During the Arctic winter, there is a persistent contrast between the multiyear ice and first-year ice [Kwok and Cunningham, 1994] to allow easy discrimination between the two ice types. An

example of tile ice classification map is shown in Fig. 4. Fetterer et al. [1994] evaluated the performance of this algorithm and reported that the precision of multiyear ice concentration estimates are better than 6%. Fetterer et al. [1994] and Steffan and Heinrichs [1991] also pointed out that the algorithm sometimes fails to correctly classify open water and 11N% ice due to overlap in the range of backscatter of these ice types. As an independent estimate, we evaluated the precision of our multiyear ice retrieval procedure, using ten pairs of SAR images of the same area acquired by the 3-day repeat cycle of ERS-1. The differences are less than 1% (Table 1). The results indicate that the signatures are stable at least over the short term and that the higher uncertainty observed by Fetterer et al. [1994] is probably due to a combination of spatial or temporal variability of the ice signature. The higher than normal backscatter of frost-flower covered sea ice could also be problematic due to their time-dependent signature [Kwok and Cunningham, 1993], but we expect that the fraction of this ice category to be less than the fraction of newly frozen leads, which is less than a few percent in the winter Arctic. Another limitation with this backscatter-based classification is the potential confusion between deformed first-year ice and multiyear ice especially in the region of transition between the seasonal and perennial ice zones [Rignot and Drinkwater, 1994]. Both ice types have similar backscatter and based on their analysis of aircraft SAR data, the multiyear ice concentration could be overestimated by as much as 15%. There is also the issue about flooding and then refreezing that suppresses the backscatter and causes underestimates in the multiyear ice concentration. In the next section, we address this issue more thoroughly when we analyze our seasonal SAR dataset.

#### *Ice concentration from ERS-1 SAR data in summer*

We do not estimate the multiyear ice concentration in the summer. After the onset of melt in the spring, the free water in the snow layer or bare ice surface act as a barrier to radar penetration into multiyear ice layer thus reducing the volume scattering contribution to the observed backscatter. The contrast between first-year and multiyear ice at C-band (see difference between Figs. 6e and f) is lost and there is at present no effective means for ice type classification in the summer time. In most cases, only open leads and ridges are visible

in ERS-1 SAR data of the summer ice cover, which has a range of backscatter between -17 dB and -14 dB. Open water backscatter is dependent on wind speed and is typically higher than that of the ice cover if the wind speed is above 4-5 m/s. The azimuthal look direction introduces only 1-2 dB of modulation of the backscatter at ERS-1 look angles. We estimate open water in leads by using an algorithm [Comiso and A'he: 1995] which takes advantage of the higher backscatter of wind-roughened open water relative to the ice cover. With an indication of wind speed, the thresholds are adjusted visually to discriminate between water and ice. During calm conditions ice concentrations are also derived, but the uncertainties are larger because of the decrease in contrast. The precision of our estimates are approximately 2-3% during windy conditions (above 4-5 m/s). To illustrate how effectively this technique works, Fig. 4a shows a typical summer SAR image near the ice edge, while Fig. 4b shows a color-coded version of the result of the classification technique. Since melt ponds are blended in with the backscatter of ice and snow on ice floes, the melt ponds are classified as ice in our algorithm. However, sub-resolution leads are not accounted for, for the same reason and cause errors in the analysis. There does not exist in the observational literature the fraction of lead area covered by leads that are not resolved by the SAR data used in this analysis. Lindsay [Personal Communication, 1995] measured the area contribution of leads with widths less than 100 m to be approximately 22% using Channel 3 of a Landsat TM image during April in the Beaufort. Within that image, the mean lead width is 140 m with few leads more than 500 m wide. If these statistics can be considered typical for the summer and winter, then this resolution problem would cause a 2% error in the SAR estimates in regions with 90% ice cover. More extensive observations, preferably airborne surveys, are necessary to better quantify this error.

## 4 Results and Discussion

For a quantitative comparison of the estimates from SSM/I and SAR, we divide the area into five latitude bands with intervals of 2.5° starting at 70°N. Several SAR images at the

beginning of each month from January through December 1992, covering the region shown in Fig. 2 were analyzed. The corresponding daily SSMI data within the 1001 $\times$ 111 by 100km area represented by each SAR image frame were also analyzed. Typical SSMI images for each month over the same general region are shown in Fig. 5. These images show spatial and temporal details about the ice cover and indicate stability in the distribution, especially in the winter. Co-registered total and multiyear ice concentration data derived from both SAR and SSMI are plotted in Fig. 6. The ice concentration results from both procedures were generally consistent except during the summer, while the multiyear ice concentrations differ substantially. Detailed discussion of the results are presented in the following sections.

#### *Total/multiyear ice concentration (Jan-May)*

In the winter, the total ice concentrations agree to within the uncertainty of the estimates at all latitude bands. There is almost 100% ice in the Beaufort Sea in the winter. We note that the Team algorithm occasionally provides anomalous estimates of ice concentrations that are greater than 100% during the winter when data points lie outside the region of validity in PR and GR space. This is due to variability in ice type signatures, system errors or weather effects.

The multiyear ice concentrations from the two analyses, however, are quite different. The SAR-derived multiyear ice concentrations are quite stable at the higher latitudes during this period and the variability is within the precision of the algorithm. There is no significant increase or decrease in the amount of multiyear ice except near the transition between the perennial pack and the seasonal ice zone. These multiyear concentrations are consistent with ice kinematics (discussed below) during this period and our expectation that this parameter stays fairly constant, especially in this part of the Beaufort Sea and the central Arctic. Within the two lowest latitude bands, we attribute the variability to the advection of multiyear ice and first-year ice into and out of the region of study (shown in Fig. 2) and possibly to the ridging of first-year ice. Large areas of ridged and highly deformed first-year ice have approximately the same backscatter signature as that of multiyear ice. Sample strips of

SAR imagery from this period are shown in Fig. 5. The contrast between multiyear ice and first-year ice persists throughout this period. The SAR-derived multiyear ice concentration isopleths are shown in Fig. 7. The pattern of the contours have remarkable similarity between observations which are temporally close to each other (e.g. Fig. 7a and b) and show a north to south decrease in concentration.

The Team algorithm estimates of multiyear ice concentration have substantially different spatial and temporal distributions than those of SAR data (Fig. 8). The Team algorithm results as shown in Fig. 6 also indicate a trend of decreasing multiyear ice concentration at the higher latitude bands. For example, between 75°N and 77.5°N there is a greater than 30% decrease in the multiyear ice concentration between January and May. The ice cover in this region computed from monthly velocity fields (between September 1, 1991 - April 1, 1992; see Fig. 9) is actually slightly convergent (0-10%) which would yield an opposite result. With a mean velocity of 2 cm/s, the total displacement of the ice is less than 240 km, much smaller than our region of study. It is difficult to explain this trend from the perspective of ice cover divergence or a net advection of multiyear ice out of our study region. The SSM/I map of multiyear ice concentrations of the Arctic Ocean for the months of January and April and their differences are shown in Fig. 10. These synoptic maps show a general decrease in multiyear ice between the two observations. We also note that the initiation of this decrease occurs earlier in lower latitudes. We hypothesize that this decrease is due to the modification of the snow layer over multiyear ice by insolation, which is a latitude and time dependent phenomenon. *Hofer and Matzler* [1980] observed that the radiometric brightness of a snow layer is very sensitive to the volumetric moisture content. Even at sub-freezing temperatures, a very small increase in the snow wetness, in the 0 to 0.5% range, can cause a large increase in the observed brightness temperature (over 100°K). So we expect that the radiometer at 37 GHz and 19 GHz to be extremely sensitive to environmental conditions which cause modification of the snow layer. Of course, the actual observed magnitude of these changes will be modulated by the extent of the surface types within the footprint of the SSM/I sensor. In the Arctic winter, the physical characteristics of the multiyear ice should

be fairly stable and should have a very stable signature. Barring any atmospheric effects, the changes on the surface of the ice or the snow layer are the primary factors responsible for the observed seasonal variability in the multiyear ice concentrations (see Fig. 2, *Rothrock and Thomas* [1993]). If our hypothesis is correct, we expect to see a reverse trend (i.e. an increase in the multiyear ice concentration) in the late fall, which is indeed the case as we shall discuss later.

The SAR estimates of multiyear ice is higher than that from the Team algorithm. We discuss this below in the context of the character of the ice cover at the end of the summer.

#### *Total ice concentration (June-September)*

Neither the Team algorithm nor the SAR algorithm provide estimates of multiyear ice in the summer, so only a comparative analysis of total ice concentrations from the two approaches is provided here.

*Comiso and Kwok* [1995] provide a more comprehensive analysis of the differences between active and passive observations for this summer period. After the onset of melt in spring, there is a gradual increase in the area fraction of open water. The SAR-derived ice concentrations are typically higher than that of the Team algorithm estimates and the differences are more pronounced at lower latitudes. A possible cause of this [discussed in *Comiso and Kwok*, 1995] is the contribution of meltponds to the open water estimates. Water in meltponds have the same passive microwave signature as that of water in open leads causing an underestimate of ice concentration. The larger difference in the lower latitude bands may be indicative of the latitude dependence of meltpond fraction. We note again that the SAR estimates are biased toward over-estimation of ice concentration because sub-resolution open leads are most likely classified as ice in the summer time. We do not know, in the current observational literature, the relative area contribution of sub-resolution leads and meltponds in the summer. If the contribution is small as we discussed earlier, for meltpond concentrations of 20-30% [*Romanov*, 1993] the meltponds would seem to be the dominant factor

which reflect the microwave signatures. In other words, the underestimation of the Team algorithm is more significant than the bias introduced by small leads. These biases can only be resolved with high resolution aerial survey.

To gain insight into the discrepancies in the summer ice concentration retrievals, total ice concentration was also derived using the Bootstrap algorithm [Comiso, 1995]. A comparison of the two SSM/I results (Fig. 11) shows that the Bootstrap algorithm estimates are typically higher than those of the Team algorithm. This is mainly because the tie-points used in the Bootstrap algorithm are adjusted to account for changes in surface emissivity during spring, mid-summer, and early autumn. However, this procedure is similarly confounded by melt ponds and values are still lower than those of SAR [Comiso and Kwok, 1995].

#### *Total/multiyear ice concentration (September-December)*

At the end of the summer, the surviving ice from the previous spring becomes multiyear ice. The SAR results show that the multiyear ice concentration in early October is roughly equivalent to the SSM/I-derived ice concentration at summer's end. Based on the SAR analysis, the ice cover seems to be fairly compact with high concentrations of multiyear ice at all latitude bands. In the following months, the concentration decreases (especially at the lower latitudes) and returns to a level comparable to that of the previous winter. We attribute this decrease to a convergence in the ice cover in the summer followed by a divergence of the ice cover in November and 1 December. Indeed, the monthly velocity fields (between April 1 - September 1, 1992; see Fig. 9) also indicate a convergence of the ice cover in this region of approximately 10-20% in the lower latitudes and divergence of a smaller magnitude in the fall. The openings in the ice cover in November can be easily observed in the SAR image strips shown in Fig. 6. The highly compact ice cover (high ice concentration) can be seen in the images shown in Fig. 12a and 12b. At this time, the ice cover seems to be composed of primarily multiyear ice with low first-year ice concentration. The high backscatter in the leads are from wind-roughened open water. In October, the ice cover has low first-year ice concentrations whereas in December the characteristic first-year ice signature (lower

backscatter) is more evident due to the thickening of the ice in the open leads created in the previous months. The ice cover attains a backscatter character, in terms of multiyear ice and first-year ice concentrations, that is similar to that of the previous winter (compare Fig 6a. and Fig. 61).

There are large differences (about 50%) between the ice concentrations at the end of the summer and the multiyear ice concentration during the subsequent winter as estimated from the Team algorithm. Such a mismatch may be due to the growth of new and young ice during the summer. This would have to occur simultaneously with the melt of a large percentage of multiyear ice. From the time sequence shown in Fig. 5, it is difficult to explain how melt and freeze-up of such magnitude could occur in the region. Our expectation is that the amount of multiyear ice should remain fairly constant especially in the higher latitudes in the central Arctic. This seems to support our hypothesis (discussed above) that the snow cover could be responding to environmental conditions or a decrease in shortwave input which causes a variability in the brightness temperature signature of multiyear ice.

Also, there is a large difference between multiyear ice concentration estimates from the SAR and the Team algorithms. The differences are likely due to the spatial variations in the emissivity of sea ice in the Arctic region [Carsey, 1982; Comiso, 1983]. One factor which causes such spatial changes in the emissivity is meltponding since frozen meltponds are known to have emissivities of first year ice [Grenfell, 1992]. This can be a substantial effect since 20-30% of the summer ice have been observed to be ponded [Tucker, private communication, 1994]. Another factor could be unusually thick snow cover in some areas which can cause flooding (and subsequent refreezing) at the snow ice interface. Such effect causes the snow/ice interface to be saline and the emissivity of the ice floe to be similar to that of first-year ice.

Could the SAR analysis overestimate multiyear ice concentration? It has been suggested [Rignot and Drinkwater, 1994] that deformed first-year ice has backscatter similar to that of multiyear ice in single polarization C-band datasets like P, RS-1. If this is the case, then the



SAR winter algorithm would certainly overestimate the multiyear ice concentration. But we argue that, due to deformation of the ice cover, the amount of deformed ice should increase as the winter wears on resulting in a gradual increase in the estimated multiyear ice concentration. Indeed we do not observe such trend, at least not within the level of uncertainty of the estimates. It is possible that deformed first-year ice<sup>are</sup> piled onto the multiyear ice and therefore not increase the concentration of multiyear ice even though the polarimetric radar records a surface type which seems to be different<sup>than</sup> that of multiyear ice. We do not know the areal contribution of this deformed first-year/multiyear ice surface type. If this area] fraction of this surface type is significant, it would contribute to an underestimation of multiyear ice in the passive microwave retrieval algorithm.

### *Comparative Study of the Signatures*

The multiyear ice concentrations as inferred from SSM/I data with the Team algorithm make use of gradient and polarization ratios. To gain insight into possible causes of disagreements between passive microwave and SAR multiyear ice data, we show scatter plots of the gradient and polarization ratios versus SAR backscatter (in dB) in Fig. 13. Data from the entire Beaufort Sea study area and also from different latitudinal bands indicate that the gradient ratios vary considerably while the polarization ratios are basically constant, for most of the data points. The multiyear ice concentration derived from passive microwave is thus dependent mainly on the gradient ratios.

At the latitudinal band between 70°N and 75°N, the gradient ratios are shown to be inversely proportional to the SAR backscatter. Between 75°N and 80°N, the data points do not appear related and are basically random. Between 80°N and 85°N, the gradient ratio varies quite a bit while the SAR backscatter signatures were almost, constant. The data points (between 80°N and 85°N) make it apparent why multiyear ice concentrations derived from the two sensors are different. In this case, the mean SAR backscatter was close to -9.3 dB while the gradient ratio varied between -0.063 to -0.098. A similar set of plots for the gradient ratios are shown in Fig. 14 but this time, multiyear ice concentration from SAR is used instead of

SAR backscatter. The plot for all regions shows the non-linearity in the relationship. At the latitudinal bands between 70°N and 75°N, the gradient ratio does not appear to be sensitive to multiyear ice concentrations between 0 to 60%. Between 60% and 90%, a strong linear relationship is apparent, but after 90%, the gradient ratio is still strongly varying while the SAR multiyear ice concentration was almost constant at about 95%.

The gradient ratio is the ratio of the difference of the vertically polarized 19 GHz and 37 GHz data and the sum of the same set of data. Plots of 19 GHz and 37 GHz data versus the SAR backscatter are shown separately in Figs. 13C and 13d, respectively. Data from the 19 GHz channel can be seen to be linearly related to the SAR backscatter at all latitudinal bands. At 80°N to 85°N, the data indicate that both brightness temperature and backscatter are well-defined. It is thus apparent that the use of 19 GHz alone to obtain multiyear ice concentration could provide results that are more consistent with the SAR data. The scatter plot of 37 GHz versus the SAR backscatter also show approximately linear relationships but it is clear that within the latitudinal range from 80°N to 85°N the distribution of data is similar to the gradient ratio versus SAR distribution.

The good correlation of 19 GHz data with the SAR data brings in the question of whether snow cover is partly a reason for the lower values in the multiyear ice concentrations derived from passive microwave versus those from SAR. The SAR and 19 GHz data are not as sensitive to snow as the 37 GHz data. While volume scattering in the multiyear ice may still be the dominant mode of scattering that enables discrimination of first year ice from multiyear ice, the 37 GHz data may also reflect scattering of the 0.8 cm radiation with snow cover. Radiative transfer modeling studies of snow indicates that this effect is not negligible.

## 5 Summary/Discussion

*Team Algorithm Estimates - Summary*

over the annual cycle, the total ice concentration remained fairly high in our region of study. From the Team algorithm estimates, we observe a significant decrease in the amount of multiyear ice (almost 40%) between January and spring melt and a slower increase in the amount of multiyear ice between September and December. We hypothesized that these trends can be explained by the cycle of insolation on the snow layer at the beginning and the end of winter. The multiyear ice concentration at freeze up is much lower than the ice concentration at the end of summer, an inconsistency in the analysis which suggests an underestimation of multiyear ice in the winter time. Meltponds and other surface effects seem to contribute significantly to the underestimation of ice concentration in the summer.

Why would the Team algorithm underestimate multiyear concentration? One possible reason is the low values of reference brightness temperatures of multiyear ice used by the algorithm. Because of the large variability of the emissivity of multiyear ice, the reference brightness temperature of multiyear ice appropriate for the entire Arctic region is difficult to establish. Another reason is having signatures similar to those of first-year ice. Some observations have shown that refrozen meltponds can have signatures of first-year ice. Also, the snow/ice interfaces of previously flooded multiyear ice floes could have signatures of first-year ice because of relatively high salinity at the surface. Furthermore, second year ice may have different emissivity than other types of multiyear ice, as has been previously observed.

### *SAR estimates - Summary*

The SAR analyses suggest an ice cover in the Beaufort which is rather stable, throughout a season, in terms of multiyear ice concentration. The amount of multiyear ice remained approximately constant, within the level of uncertainty of the analysis. The average multiyear ice concentration in this part of the Arctic Ocean is approximately 80%. At the end of the summer, the multiyear ice concentration is approximately equivalent to the ice concentration at the end of the summer. The analyses give a consistent view of the annual cycle.

We have analyzed the possible confusion for identification of multiyear ice in the winter

Beaufort Sea. Evidence seem to indicate (discussed in the last section) that deformed first-year ice, within the level of uncertainty, does not contribute significantly to the overestimation of multiyear ice in SAR data. The C-band radar, to first-order, is not affected by snow cover when the temperature is below freezing and much less sensitive to weather effects. The summer/winter consistency and the small fluctuations in the SAR estimates lead us to believe that these estimates to be reliable.

10

### *Multiyear ice concentration*

The significance of the multiyear ice in the Arctic Ocean can be attributed to its strong relation to the summer ice concentration [Comiso, 1990; Rothrock and Thomas, 1990]. If there are changes in the climate which cause persistent decrease in the summer ice concentration, it would be reflected in a decrease in the amount of multiyear ice in the winter. This reduction would be due to increased melt or export of ice from the Fram strait. An accurate record of the multiyear ice balance and fluctuations would be useful in understanding the relationship between climate and multiyear ice balance.

Rothrock and Thomas [1990] demonstrated that more multiyear ice is required to maintain consistency between the summer ice and winter multiyear ice concentrations. However, as they carefully indicated, their Kalman filter smoother can insist on consistency but without providing more accurate estimates if the observations are biased. That is, the estimates themselves are biased. At this point, the analysis of the SAR data offers another estimate of the multiyear ice, which seems to be consistent with the summer ice concentration. If the SAR is correct, then the Team algorithm underestimates the multiyear ice by even a larger amount than previously suggested and there is more multiyear ice in the Beaufort Sea.

### *Meltpond fraction and ice extent*

Both open water and meltponds have signature of open water and the Team algorithm does not discriminate between the two surface types. It underestimates the ice concentrations in the summer. If the meltpond concentration is 30%, then the estimates would be biased

by a similar amount. This is consistent with the differences between the SAR analysis and the Team algorithm analysis: the SAR estimates of total ice concentration is always higher than that of the Team algorithm estimates in the summer. This difference is also larger in the lower latitude bands suggesting that meltpond fraction is dependent on latitude and proximity to the coast [Romanov, 1993].

If Team algorithm underestimates the total ice concentration due to meltponds, especially in the ice margin in the summer, then the 15% ice edge would be displaced resulting in an underestimation of the actual ice cover [Comiso and Kwok, 1995].

### *Summary Remarks*

The estimates from the SAR and Team algorithms provided two fairly different views of the Beaufort Sea ice cover. The limitations of both algorithms were discussed. The differences explain some of the possible biases of these algorithms due to variability in signature as functions of wavelength and environmental conditions. Future investigations using these datasets should be cautious of possible biases of introduced by these datasets.

### *Acknowledgments*

The authors would like to thank Rico Allegrino of Hughes STX for his assistance in programming and analysis of data. R. Kwok and G. F. Cunningham performed this work at the Jet Propulsion Laboratory, California Institute of Technology under contract with the National Aeronautics and Space Administration. J. C. Comiso performed this work at the Laboratory for Hydrospheric Processes at NASA Goddard Space Flight Center. This project was supported by the NASA Cryospheric Processes Program under R. H. Thomas.

## References

- Carsey, F. D., Arctic sea ice distribution at end of summer from satellite microwave data. *J. Geophys. Res.*, 87(C8), 5809-5835, 1982.
- Cavalieri, D. J., P. Gloersen and W. J. Campbell, Determination of sea ice parameters from Nimbus 7 SMMR, *J. Geophys. Res.*, 89(14), 5355-5369, 1984.
- Cavalieri, D. J., The validation of geophysical products using multisensor data, in *Microwave Remote Sensing of Sea Ice*, Ed. F. D. Carsey, Geophysical Monograph 68, AGU, 1992.
- Comiso, J. C., Sea ice microwave emissivities from satellite passive microwave and infrared observations, *JGR*, 88(C12), 7686-7704, 1983.
- Comiso, J. C., Arctic multiyear ice classification and summer ice cover using passive microwave satellite data, *J. Geophys. Res.*, 95(C8), 13411-13422, 1990.
- Comiso, J. C., SSM/I Ice Concentrations Using the Bootstrap Algorithm. *NASA Publication*, 1[ ]-1380, 50pp, 1995.
- Comiso, J. C. and R. Kwok, The summer Arctic sea ice cover from satellite observations, [in preparation].
- Fetterer, F., D. Gineris and R. Kwok, Sea ice type maps from Alaska synthetic aperture radar facility imagery: An assessment, *J. Geophys. Res.*, 99(C11), 22443-22458, 1994.
- Gloersen, P. and D. J. Cavalieri, Reduction of weather effects in the calculation of sea ice concentration from microwave radiances, *J. Geophys. Res.*, 91(C3) 3913-3919, 1986.
- Grenfell, T. C., Surface-based passive microwave observations of sea ice in the Bering and Greenland Seas, *IEEE Trans. Geosci. Remote Sens.*, GE-24(6), 826-831, 1986.
- Grenfell, T. C., Surface-based passive microwave studies of multiyear ice, *J. Geophys. Res.*, 97(C3), 3485-3501, 1992.

- Grenfell, T. C. and A. W. Lohanick, Temporal variations of the microwave signatures of sea ice during the late spring and early summer near Mould Bay NWT, *J. Geophys. Res.*, 90(C3), 5063-5074, 1985.
- Kwok, R and G. F. Cunningham, Backscatter Characteristics of the Winter Sea Ice Cover in the Beaufort Sea, *J. Geophys. Res.*, 99(C4), 7787-7803, 1994.
- Kwok, R., E. Rignot, B. Holt and R. G. Onstott, Identification of Sea Ice Types in Spaceborne SAR Data, *J. Geophys. Res.*, 97(C2), 2391-2402, 1992.
- Kwok, R. and G. F. Cunningham, Use of Time Series SAR Data To Resolve Ice Type Ambiguities in Newly-opened Leads, *Proceedings of IGARSS'94*, Pasadena, CA, 1024-1026, 1994.
- Rignot, E. and M. Drinkwater, Winter sea ice mapping from multi-parameter synthetic aperture radar, *J. Glaciol.*, 40(134), 31-45, 1994.
- ИОИЛМОВ, И. И., *Morphometric characteristics of ice and snow in the Arctic Basin*, St. Petersburg, 1993.
- Rothrock, D. A. and D. R. Thomas, The Arctic Ocean multiyear ice balance, 1979-82, *Ann. Glaciol.*, 14, 252-255, 1990.
- Steffan, K. and J. Heinrichs, Feasibility of sea ice typing with synthetic aperture radar (SAR): Merging of Landsat thematic mapper and 111{ S-1 satellite imagery, *J. Geophys. Res.*, 99(C11), 22413-22421, 1994.
- Thomas, D. R. and D. A. Rothrock, The Arctic Ocean ice balance: A Kalman filter smoother estimate, *J. Geophys. Res.*, 98(C6), 10054-10067, 1993.
- Thomas, D. R., Arctic sea ice signatures for passive microwave algorithms, *J. Geophys. Res.*, 98(C6), 10037-10052, 1993.
- Wittmann, W. I. and J. Schule Jr., Comments on total mass budget of Arctic ice pack, *Proceedings of the Symposium on the Arctic Heat Budget and Atmospheric Circulation*, X

J. O. Fletcher, ed., 215-246, Memo. RM-5233-NSF, Rand Corp., Santa Monica, CA, 1966.



## Figure Captions

Figure 1. Expected variability of sea ice cover over an annual cycle.

Figure 2. The comparative analysis uses ERS-1 SAR data and SSMI data from the region defined by these boundaries.

Figure 3. Sample SAR ice classification map (winter). (a) The image and the ice type map. (b) The image and the ice type map 3 days later. (White = multiyear ice; blue = deformed first-year ice; green = undeformed first-year ice; red = smooth thin ice or calm open water).

Figure 4. Sample SAR classification map (summer). (a) SAR image. (b) Image classified into ice, grease ice and open water. (White = open water; blue = ice; red = grease ice).

Figure 5. View of the ice cover from SAR. (a) January. (b) February. (c) March. (d) April. (e) May. (f) June. (g) July. (h) August. (i) September. (j) October. (k) November. (l) December. The winter scenes show very stable SAR backscatter while the contrast that is typical in the winter is lost in the summer. The strips are 100 km in width and the longest strips contain up to 15 image frames (or 1500 km in length).

Figure 6. Comparisons of the total ice and multiyear ice concentrations at five latitude bands. (a) 70.0°-72.5°. (b) 72.5°-75.0°. (c) 75.0°-77.5°. (d) 77.5°-80.0°. (e) 80.0°.

Figure 7. Multiyear ice concentration isopleths of the study region. (a) Day 18. (b) Day 21. (c) Day 71. (d) Day 74. (e) Day 90.

Figure 8. Monthly-averaged SSMI multiyear ice concentration maps.

Figure 9. Mean monthly velocity and divergence calculated from wind and buoy data. (a) September 1, 1991 - April 1, 1992. (b) April 1, 1992 - September 1, 1992. (c) September 1, 1992 - April 1, 1993. (Courtesy of R. E. Moritz, R. Colony and K. Runciman, Polar Science

Center, University of Washington )

Figure 10. The difference between the Team algorithm derived multiyear ice concentration in Jan 1, 1992 and April 1, 1992. A significant decrease in the multiyear ice concentration can be observed.

Figure 11. Differences between the Bootstrap and Team algorithm-derived total ice concentration 011 Sept 5, 1992.

Figure 12. Image sequence showing the compactness of the ice cover before and after fall freeze-up. (a) 80°N. (a) 75°N. The common features between the images (where they could be identified) are marked with an 'X'.

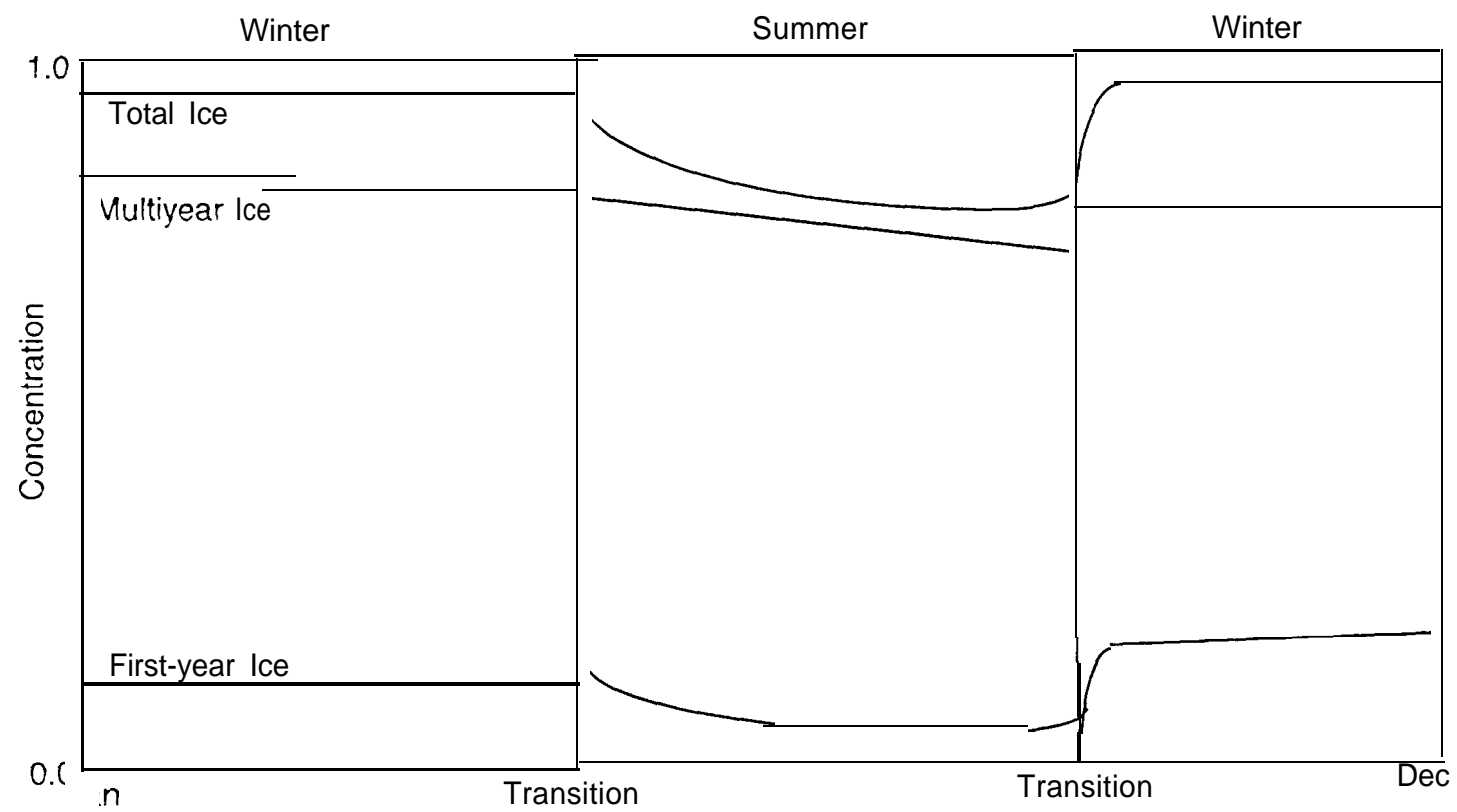
Figure 13. Comparison of SAR and passive microwave signatures at three latitudinal bands. (a) Polarization ratio vs SAR backscatter. (b) Gradient ratio vs SAR backscatter. (c) 19 GHz brightness temperature vs SAR backscatter. (d) 37 GHz brightness temperature vs SAR backscatter.

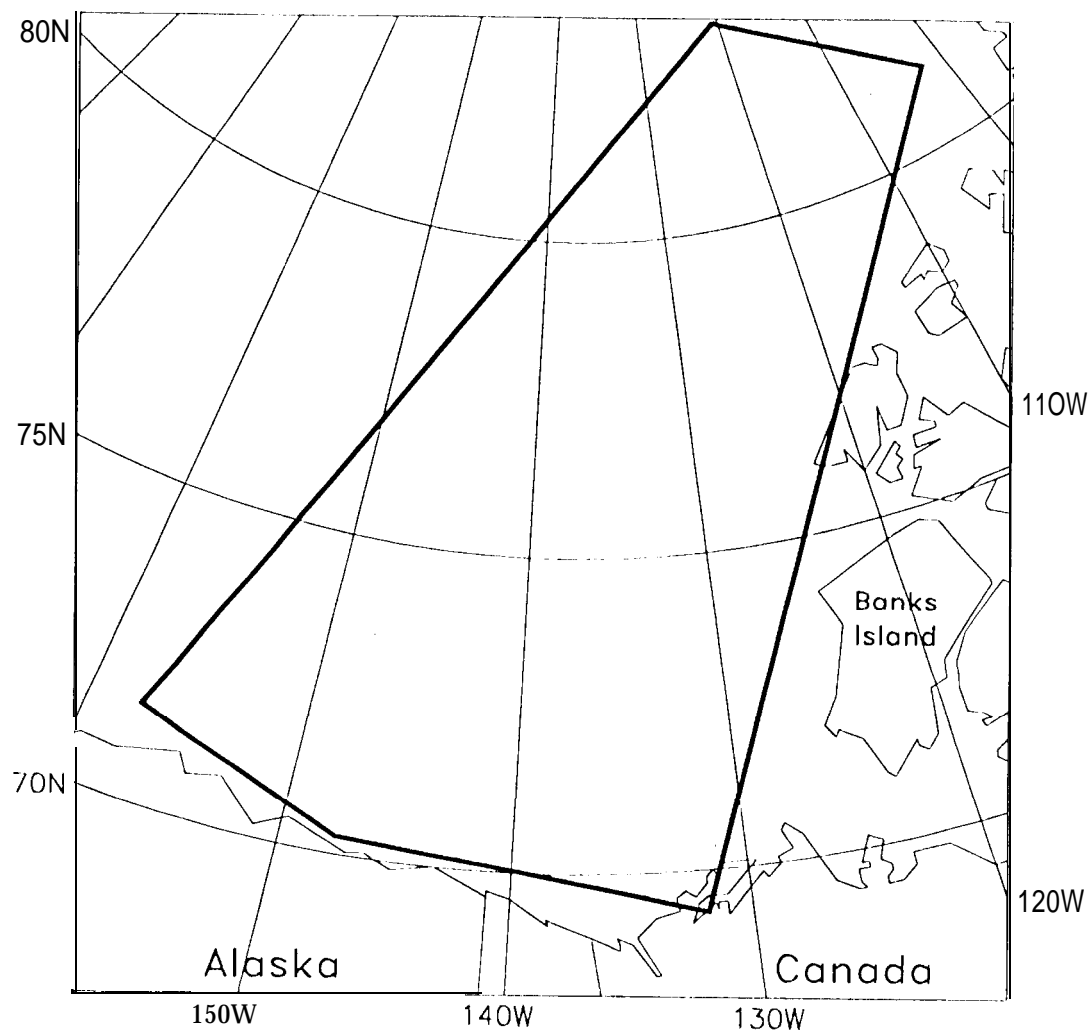
Figure 14. Scatterplot of gradient ratio at various latitude bands versus SAR multiyear ice concentration.

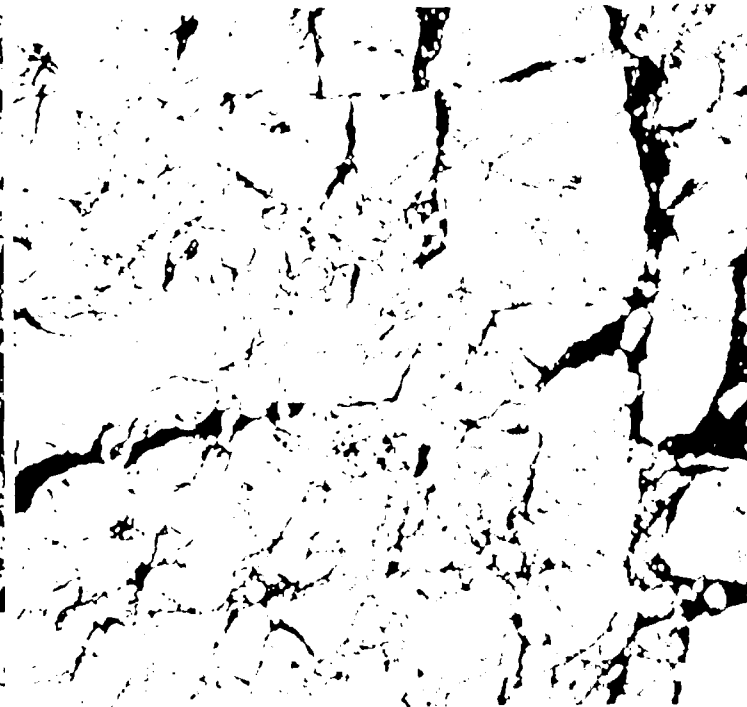
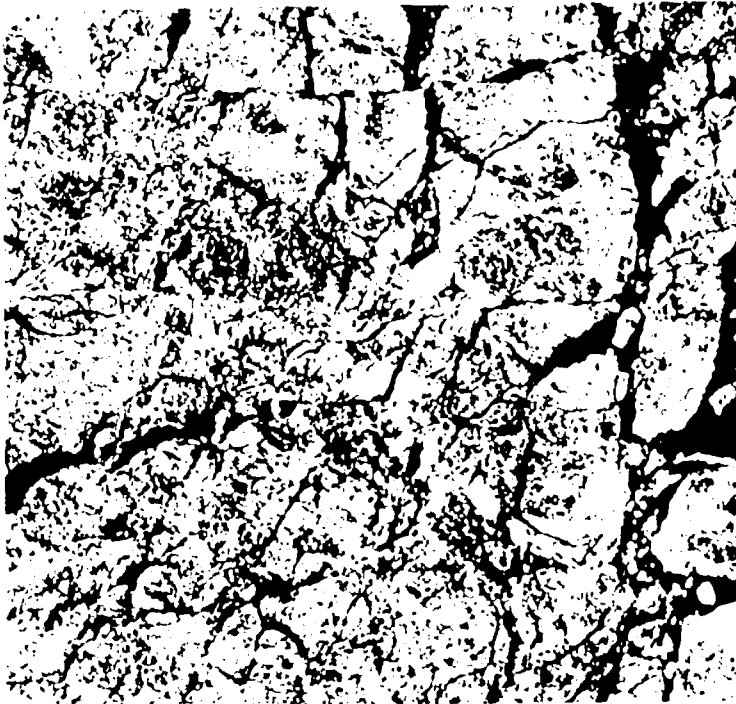
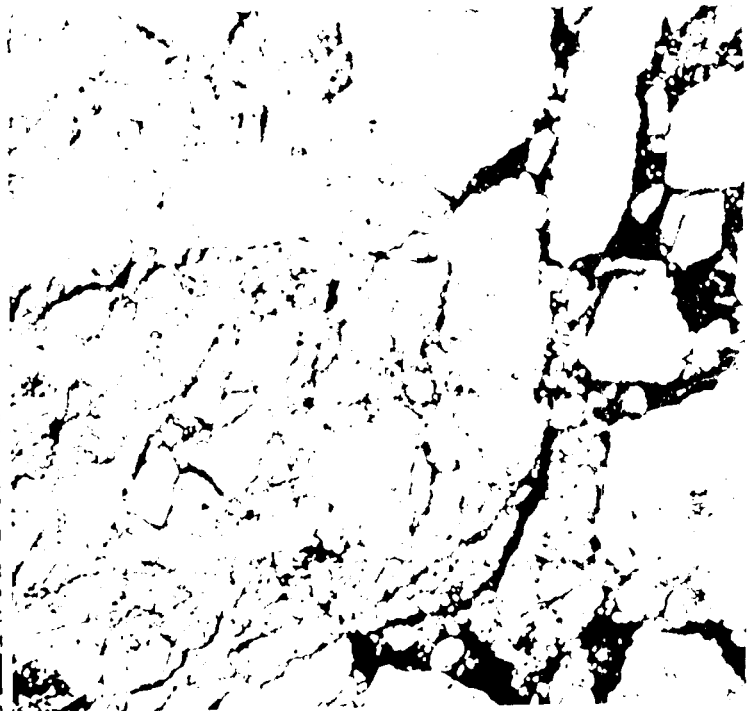
Table 1

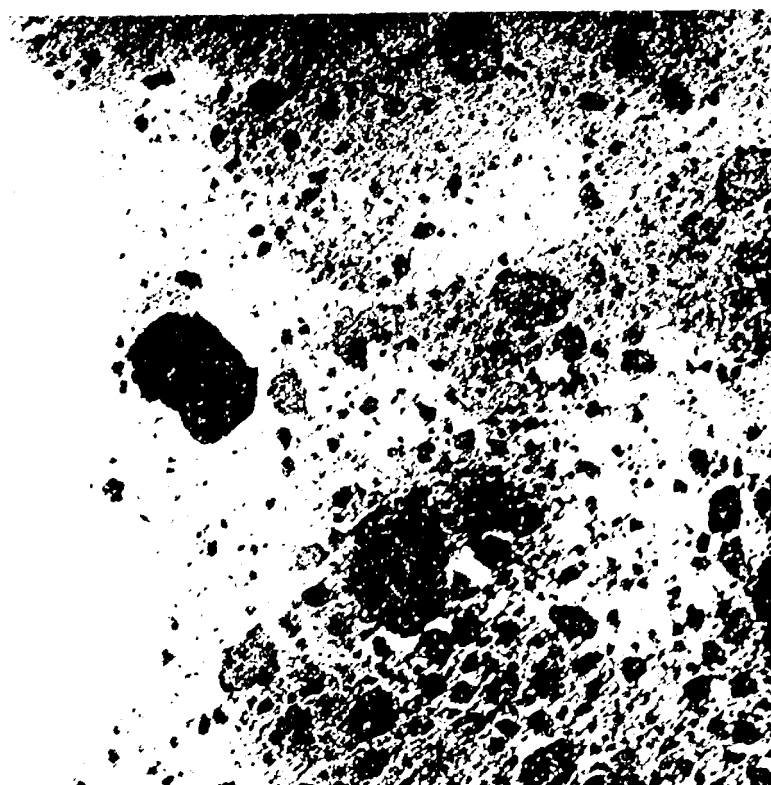
Consistence in the Classification of MY ice  
in 3-day repeat SAR imagery

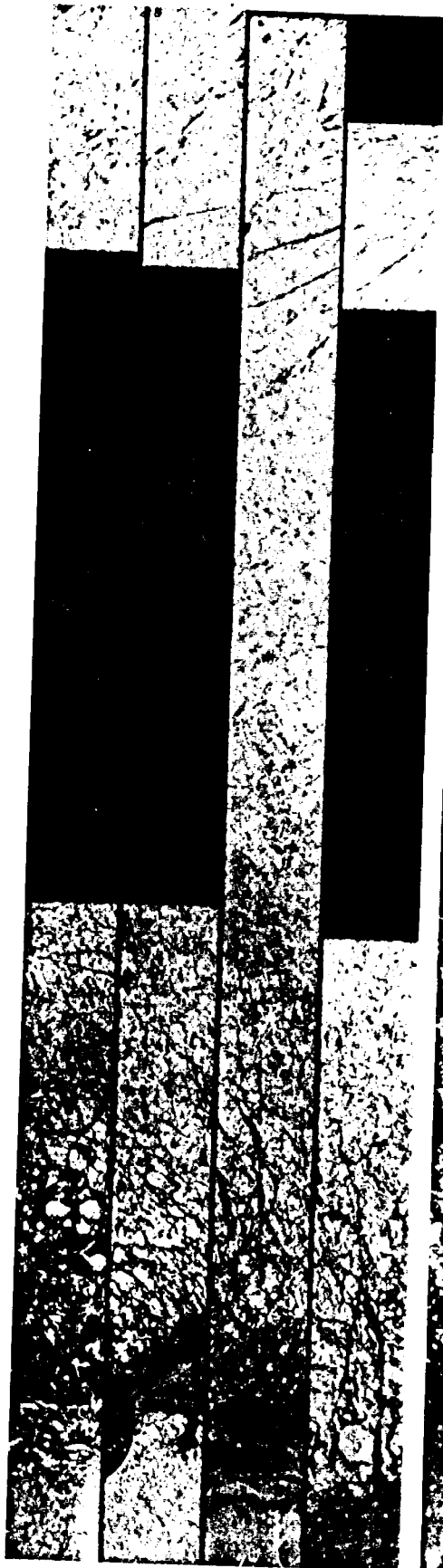
Image pair	MY concentration
3620	98.35
4092	98.29
3621	97.65
4093	97.84
11280	95.83
11955	96.16
11284	96.35
11959	96.37
11287	95.79
11962	95.83
11288	94.74
11963	94.56
11289	94.89
11964	94.61
11295	70.51
11970	70.32
13009	95.32
13726	95.96
13011	94.26
13728	94.34
RMS error	0.27



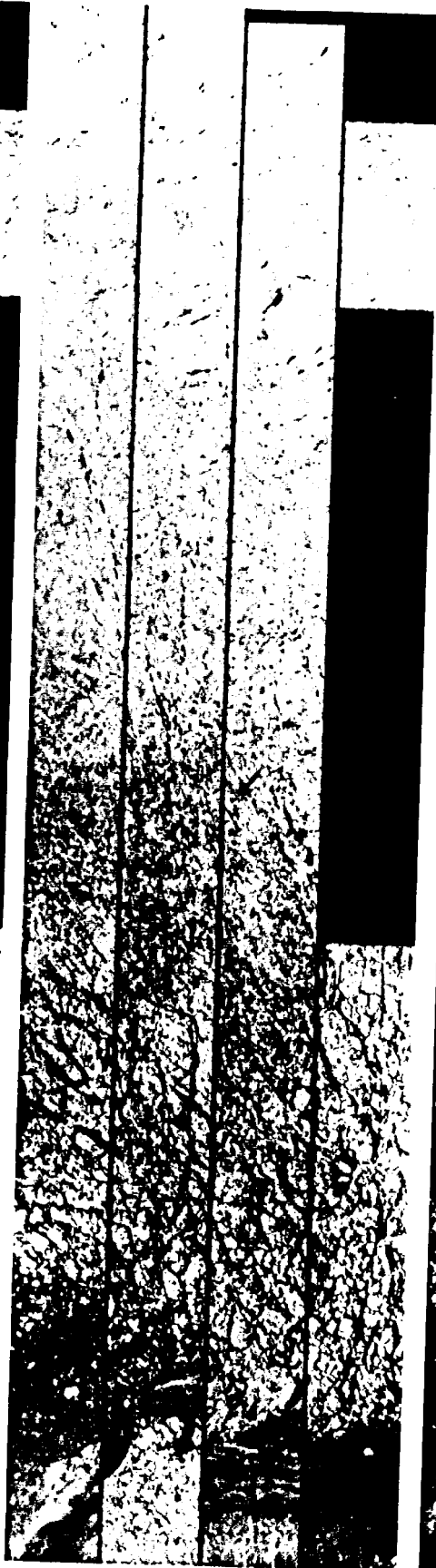




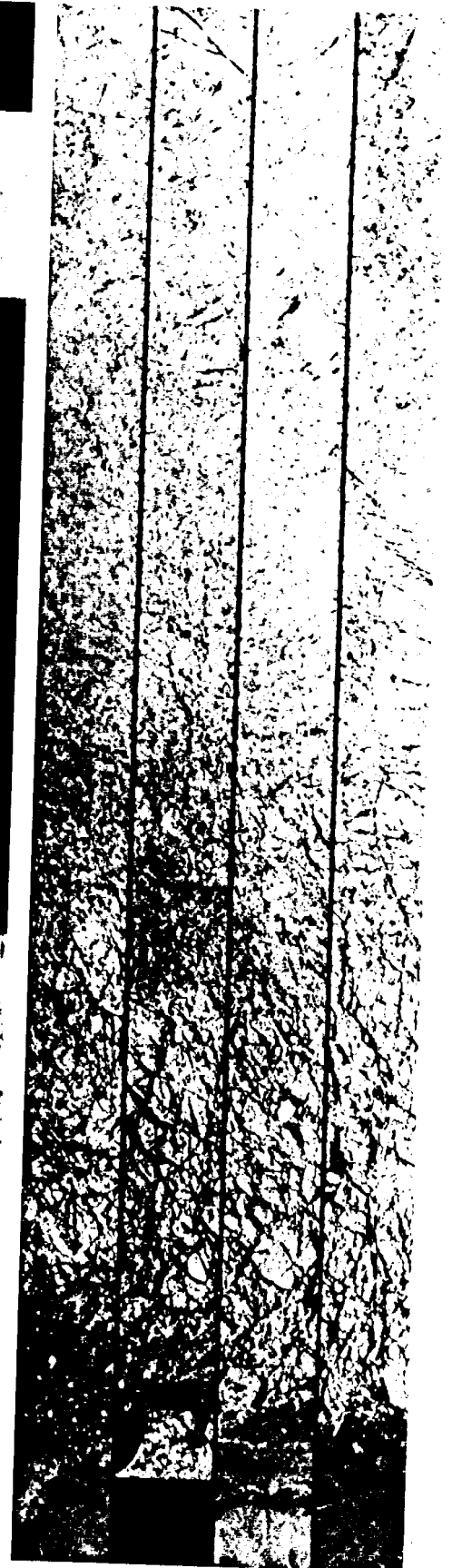




JANUARY '92

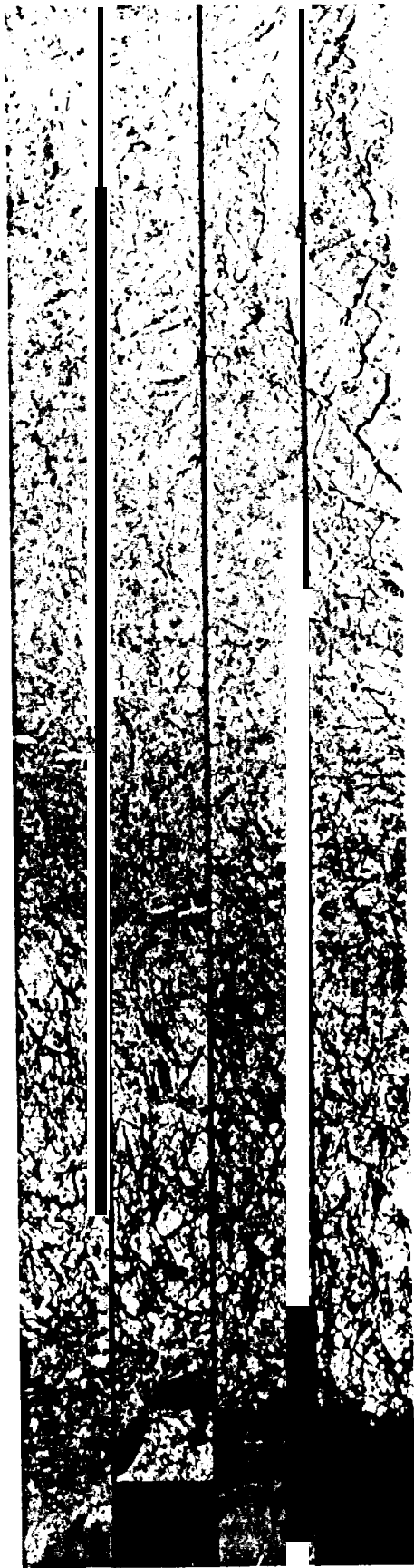


FEBRUARY



MARCH





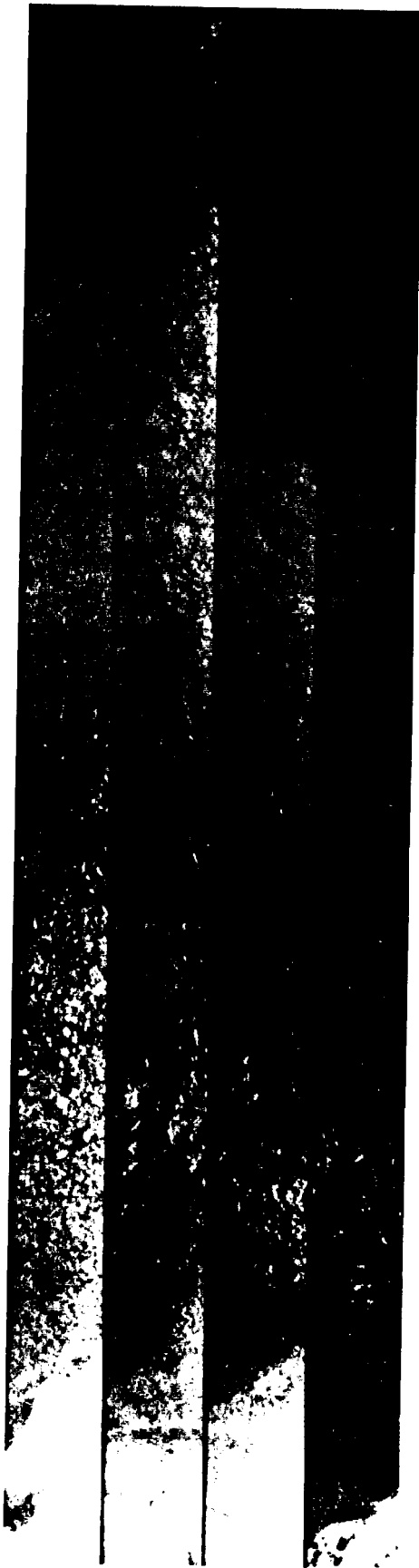
APRIL



MAY



JUNE



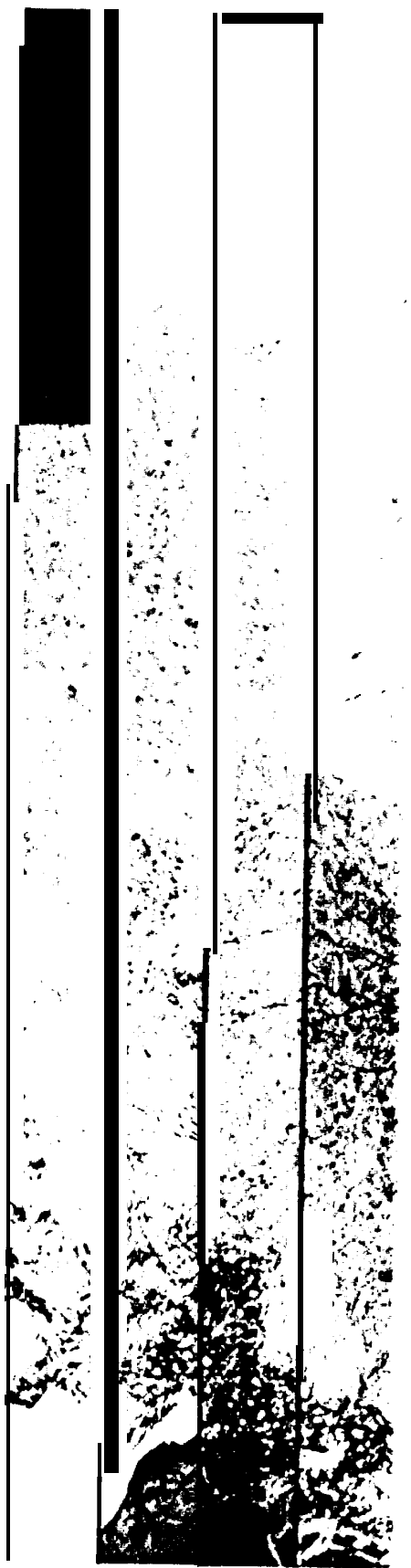
JULY



AUGUST



SEPTEMBER



OCTOBER

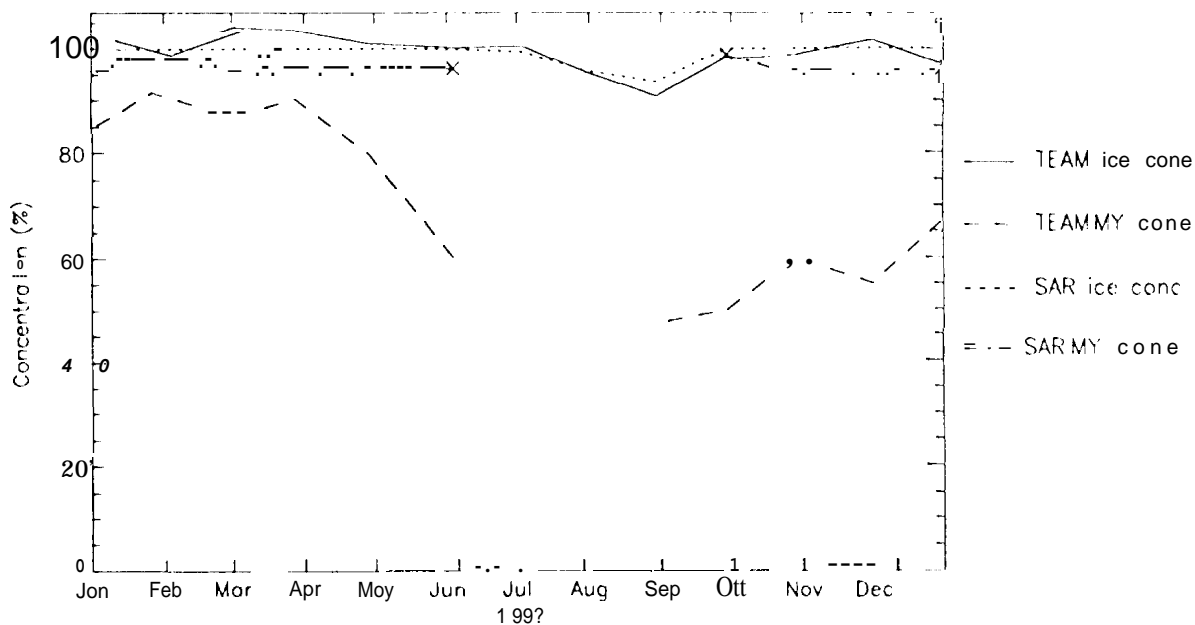


NOVEMBER

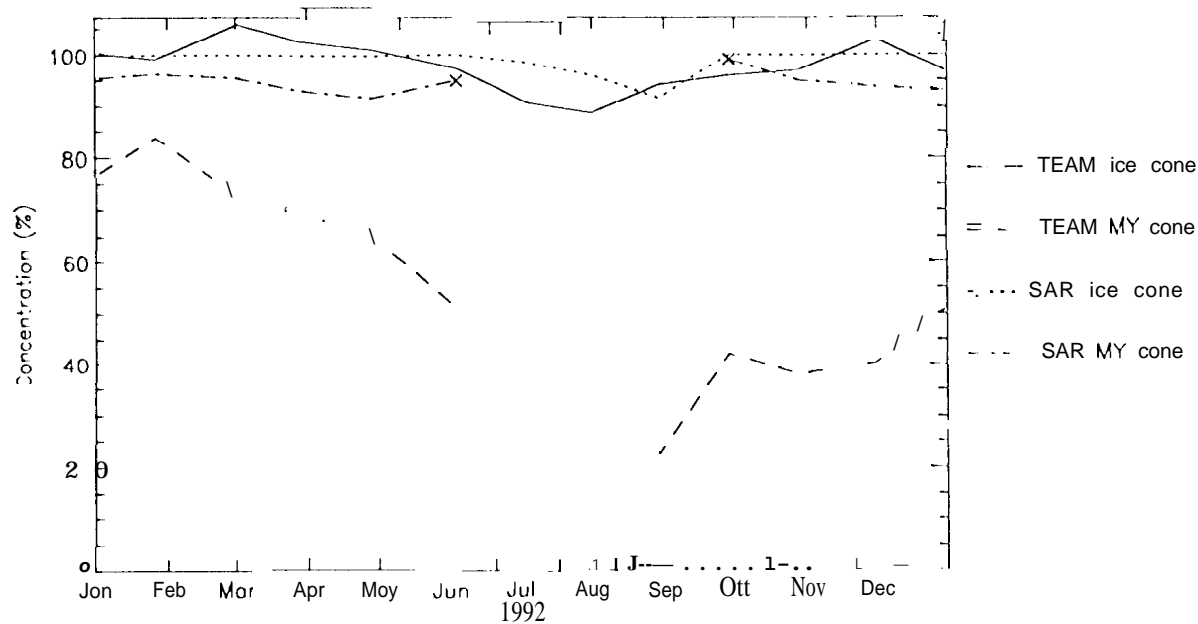


DECEMBER

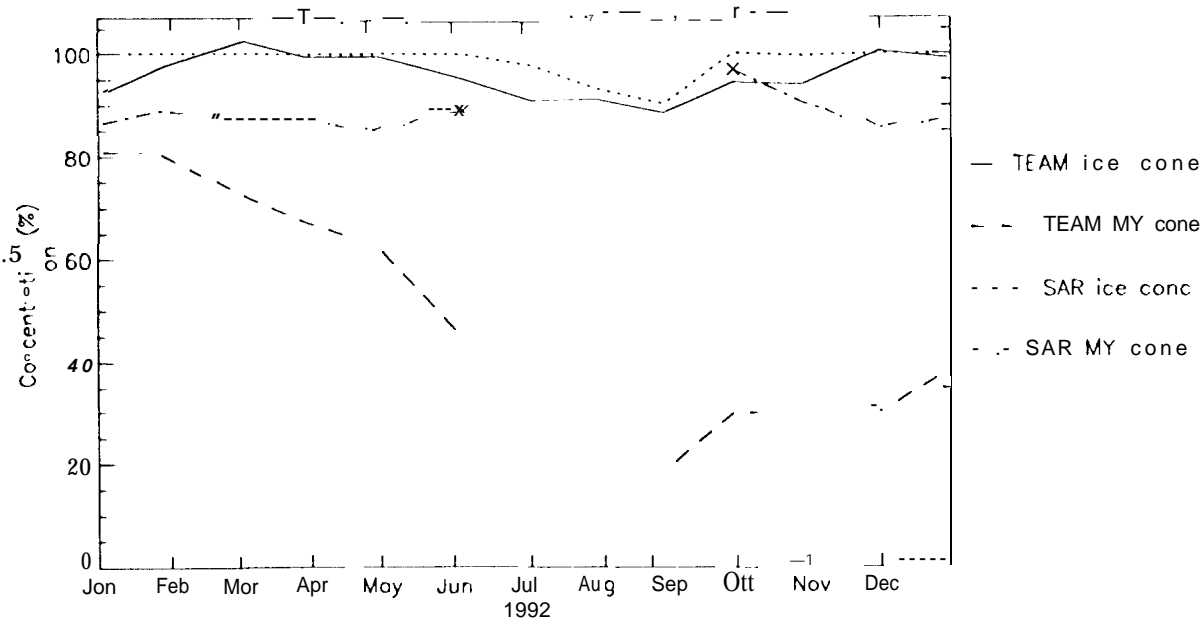
Lot. Bond:  
> 80.0



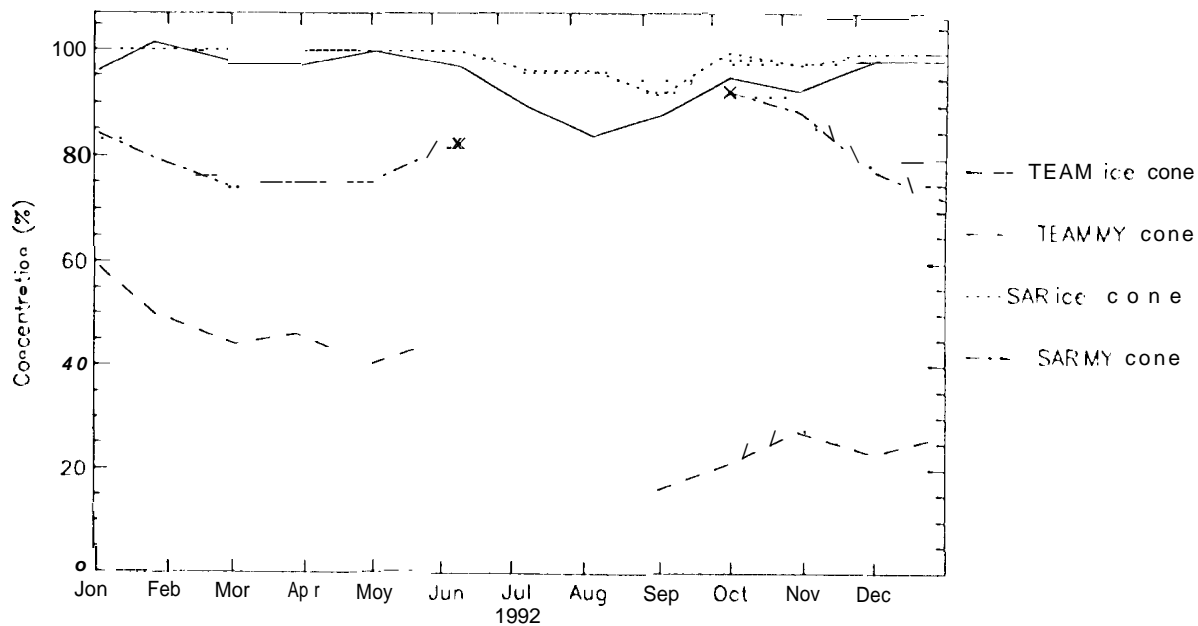
Lot. Bond:  
77.5 => 80.0



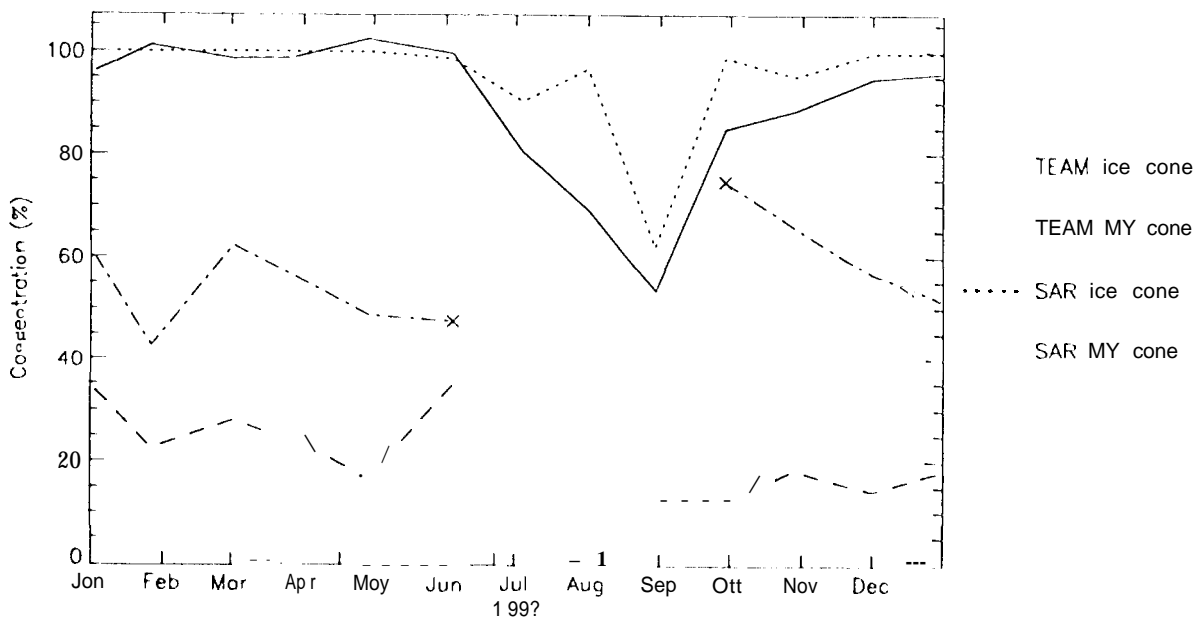
Lot. Bond:  
75.0 => 77.5



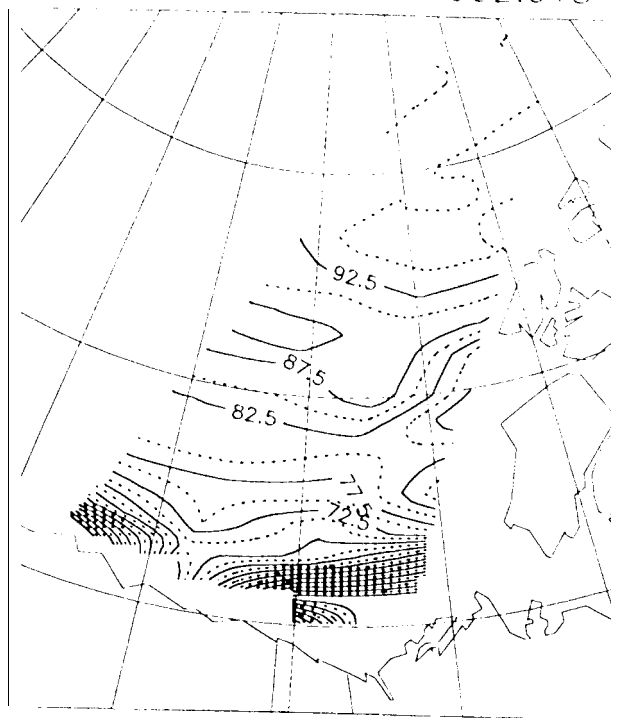
Lot. Bond:  
77.5 => 75.0



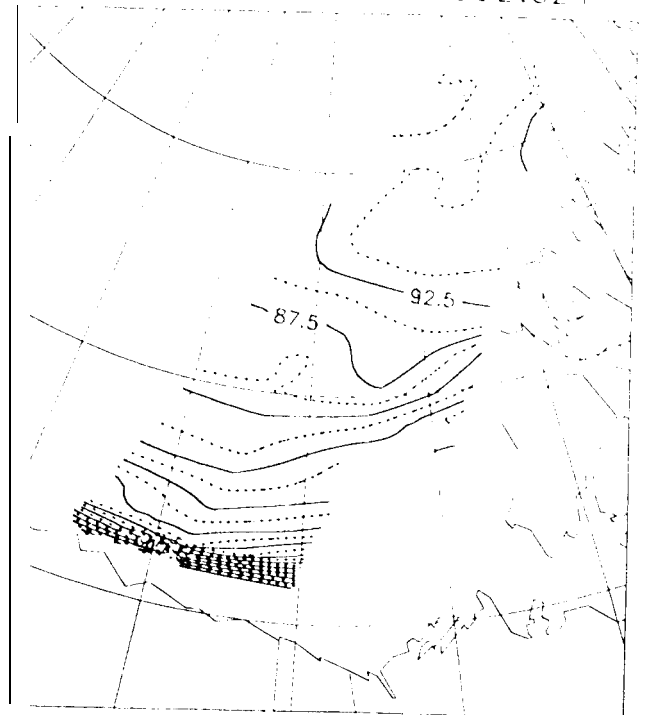
Lot. Bond:  
70.0 => 77.5



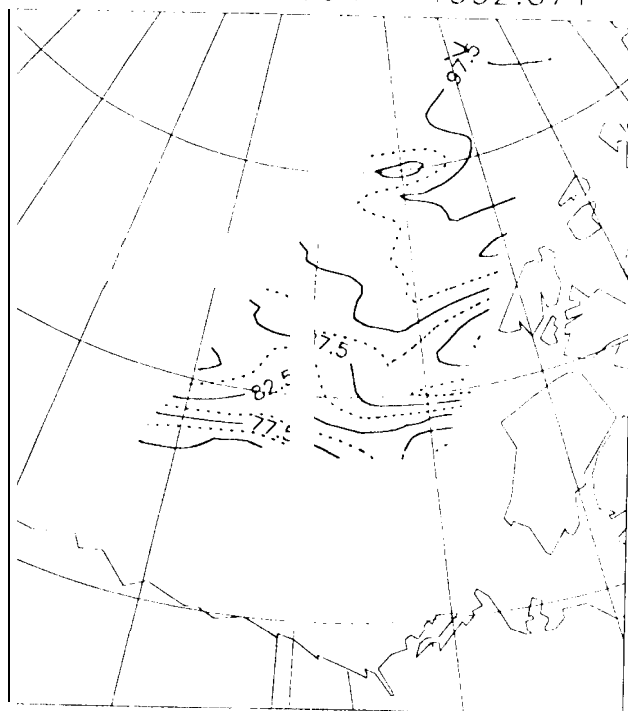
MY Concentration - 1992:018



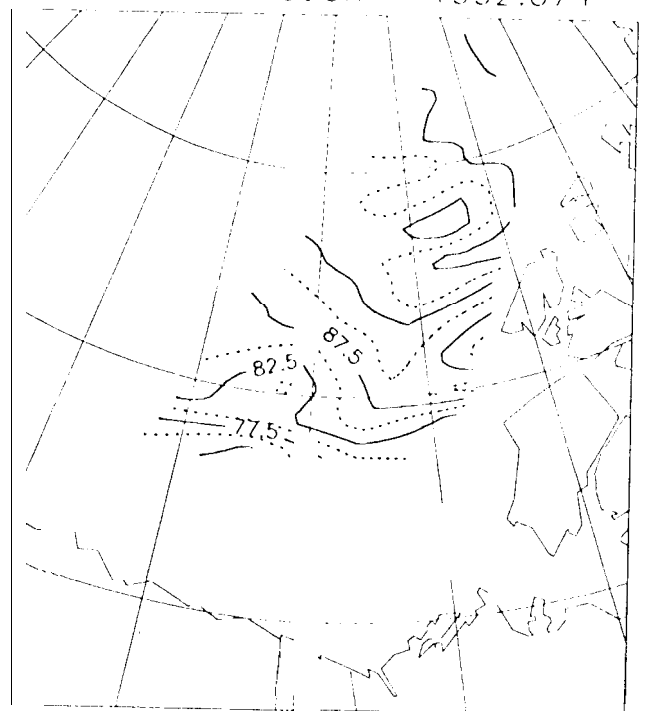
MY Concentration - 1992:021



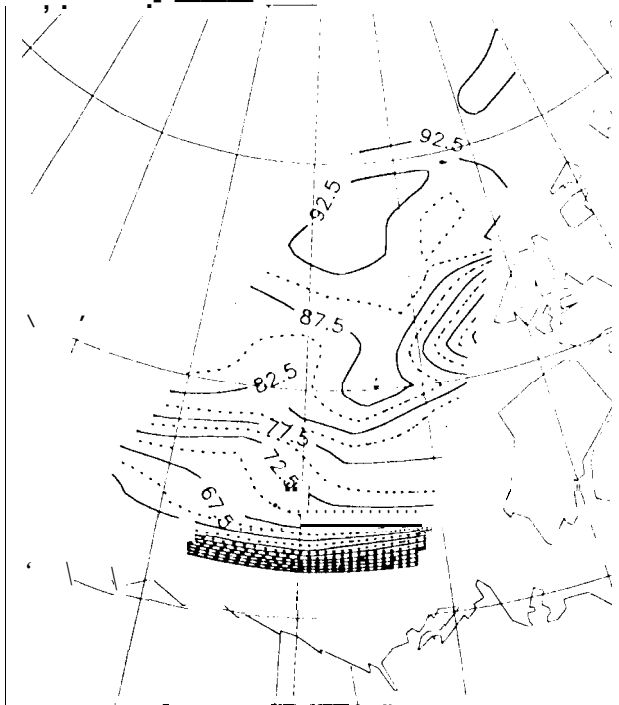
MY Concentration - 1992:071

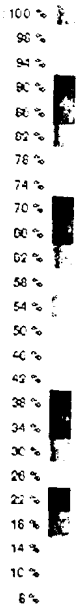
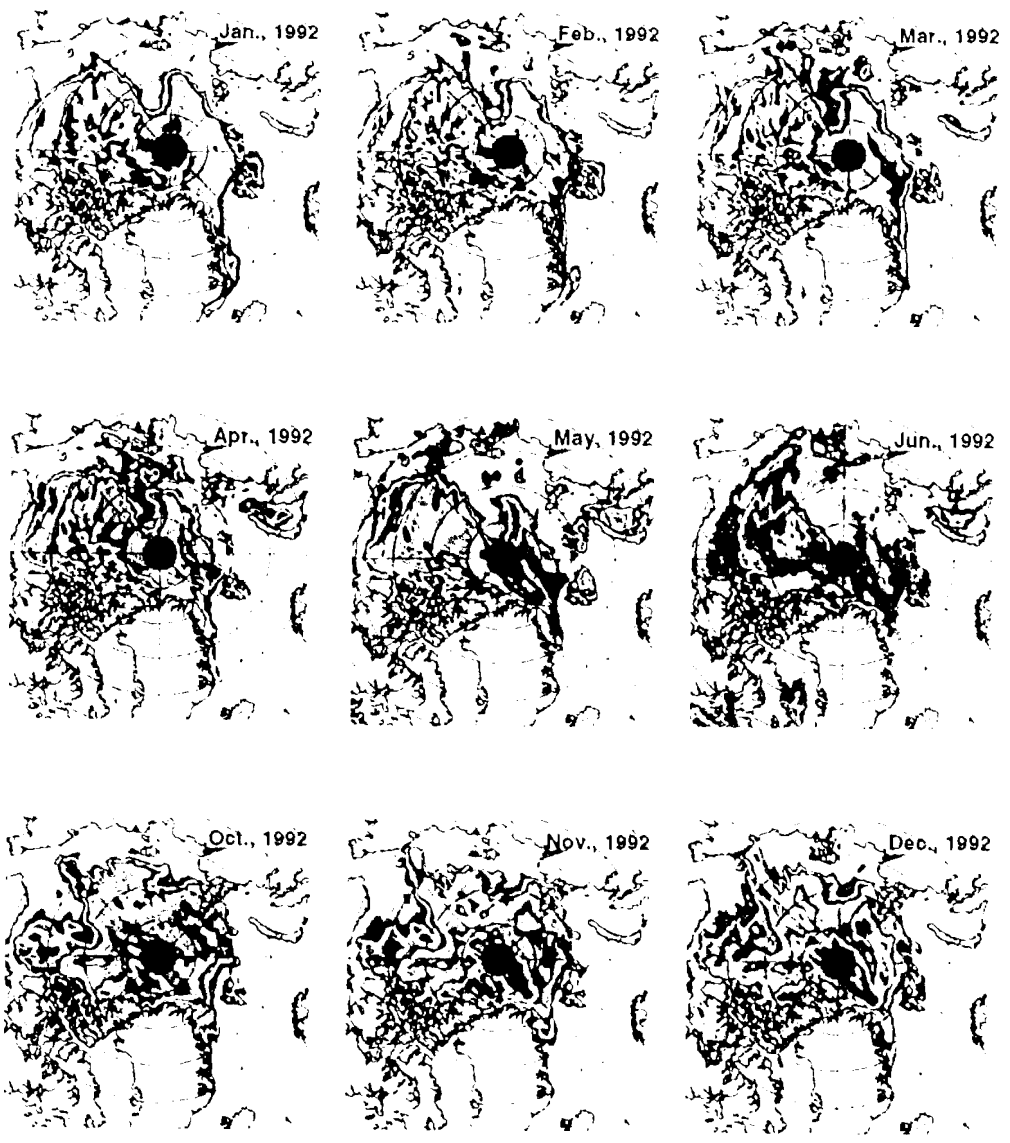


MY Concentration - 1992:074



M Y Concentration - 1992:090

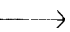


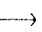





(a) Mean Ice Velocity : Sep 91-Apr 92

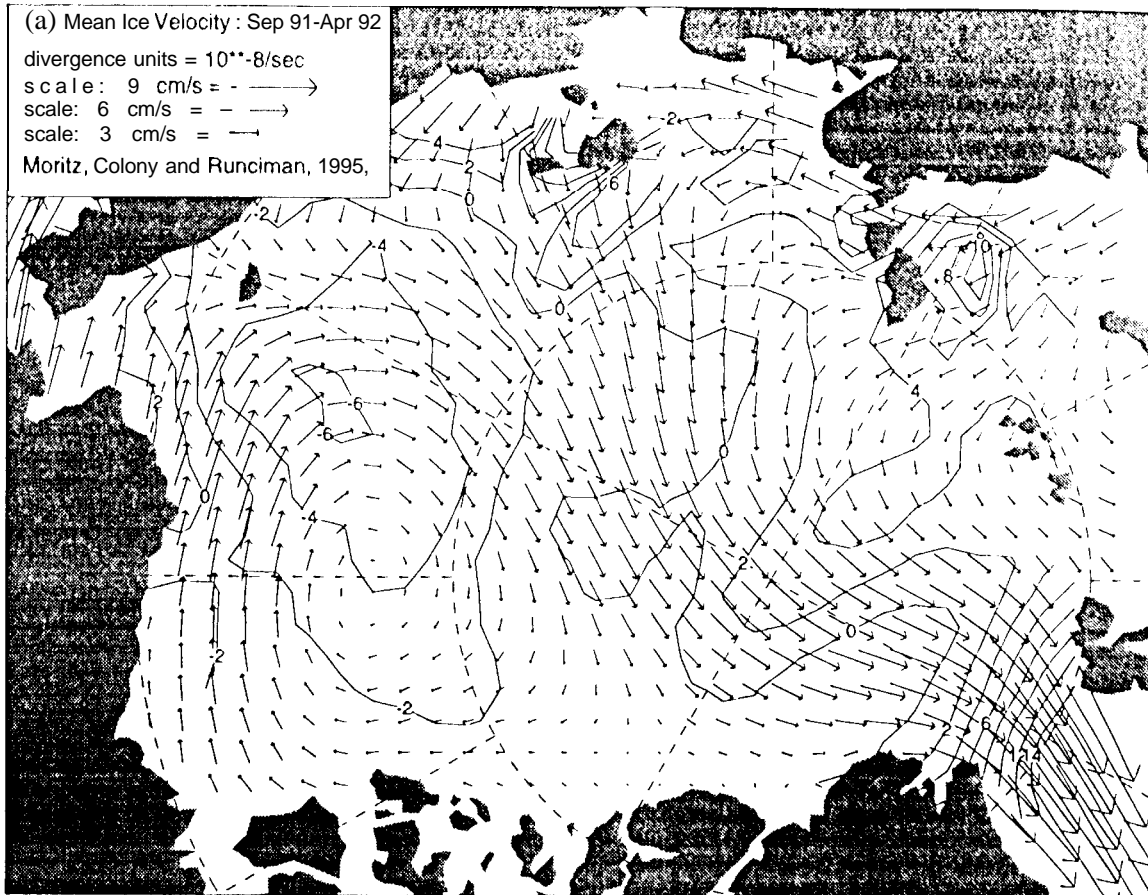
divergence units =  $10^{-8}$ /sec

scale: 9 cm/s = 

scale: 6 cm/s = 

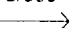
scale: 3 cm/s = 

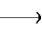
Moritz, Colony and Runciman, 1995.

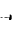


(b) Mean Ice Velocity : Apr 92-Sep 92

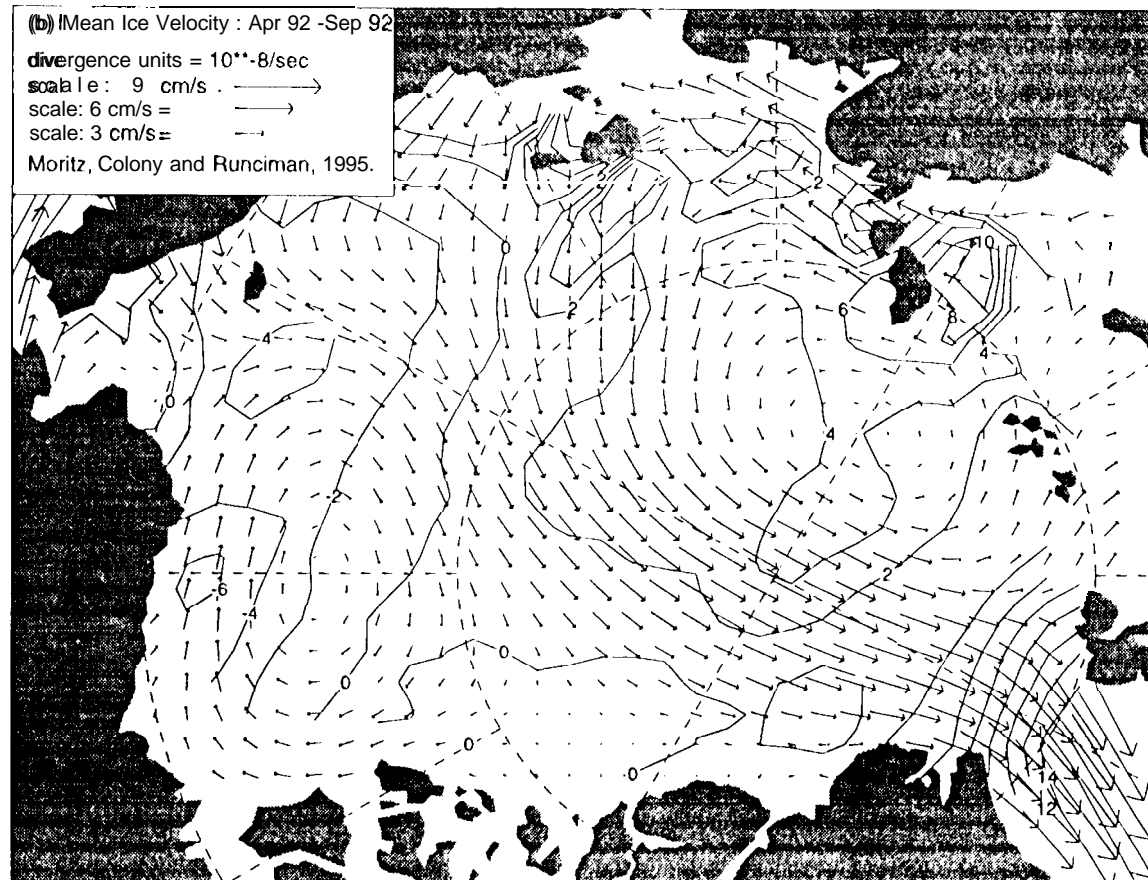
divergence units =  $10^{-8}$ /sec

scale: 9 cm/s = 

scale: 6 cm/s = 


scale: 3 cm/s = 


Moritz, Colony and Runciman, 1995.




(c) Mean Ice Velocity : Sep 92-Apr 93

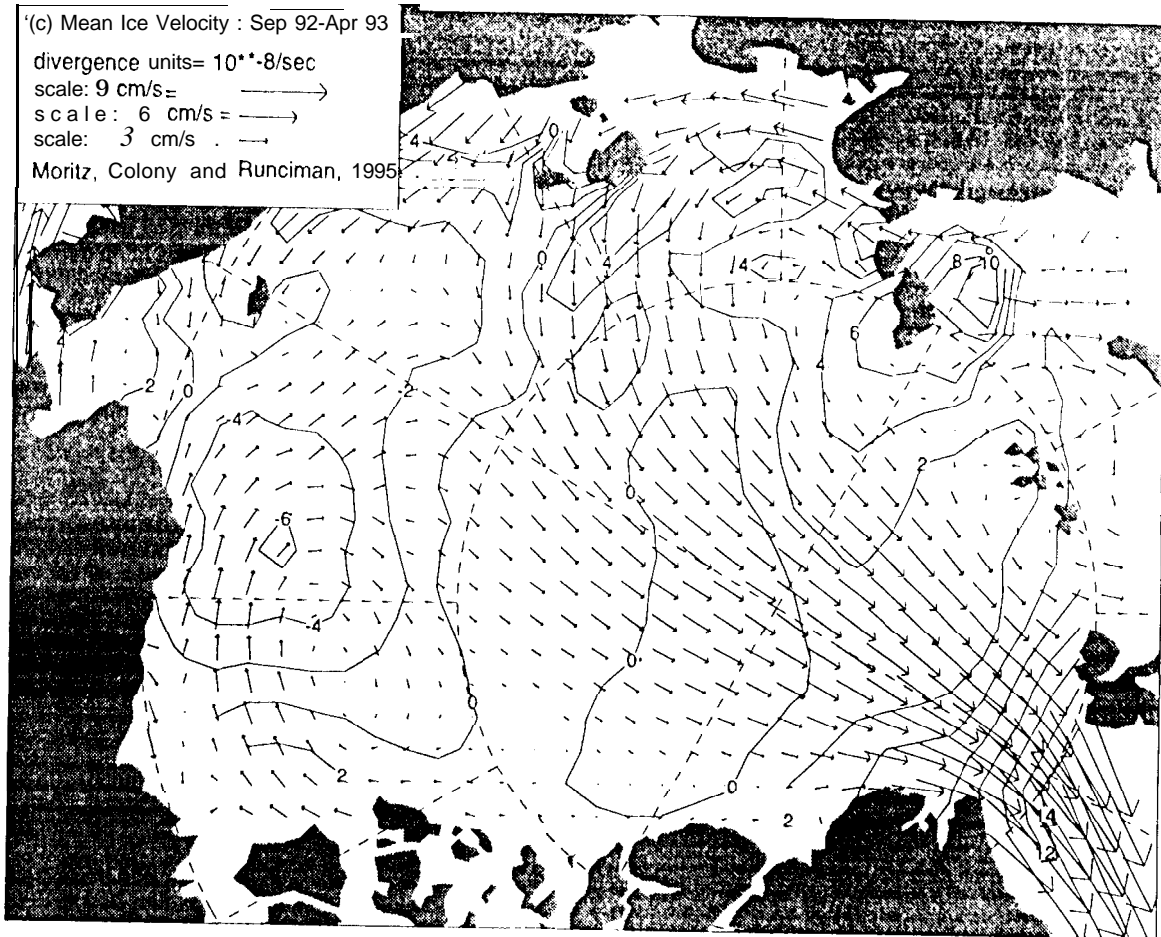
divergence units =  $10^{-8}$ /sec

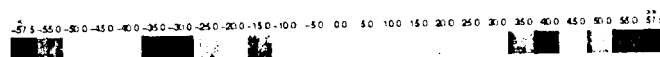
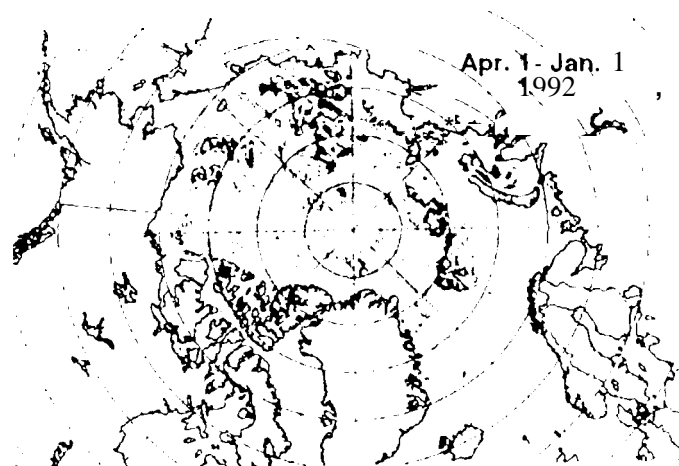
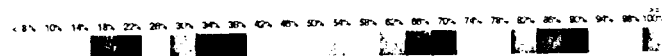
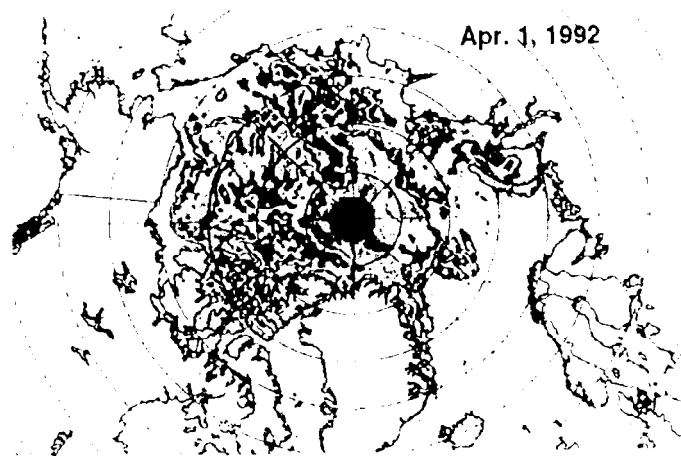
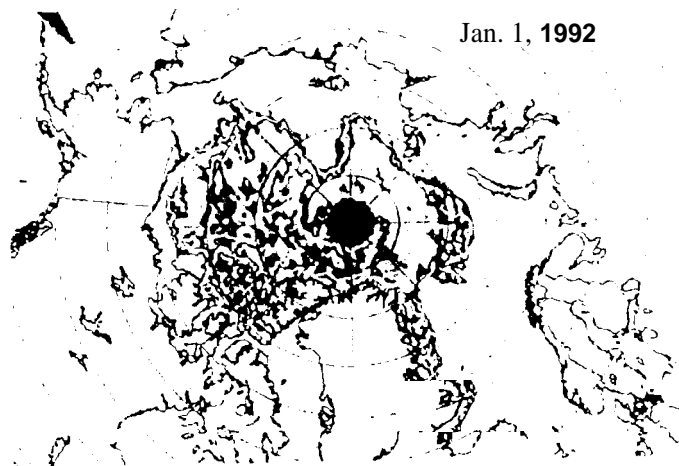
scale: 9 cm/s = 

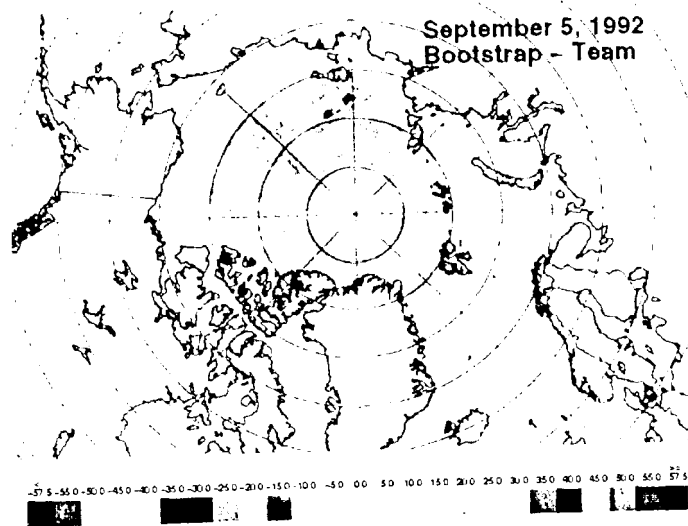
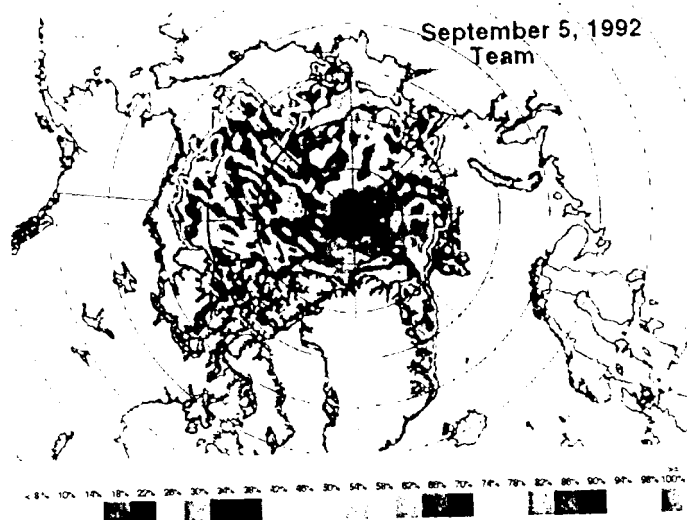
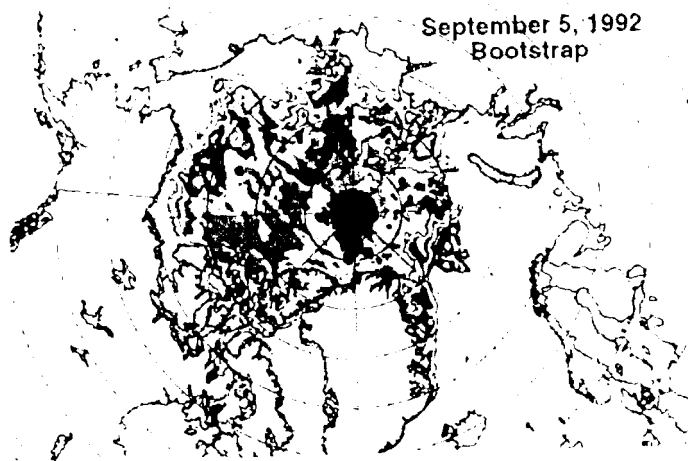
scale: 6 cm/s = 

scale: 3 cm/s = 

Moritz, Colony and Runciman, 1995

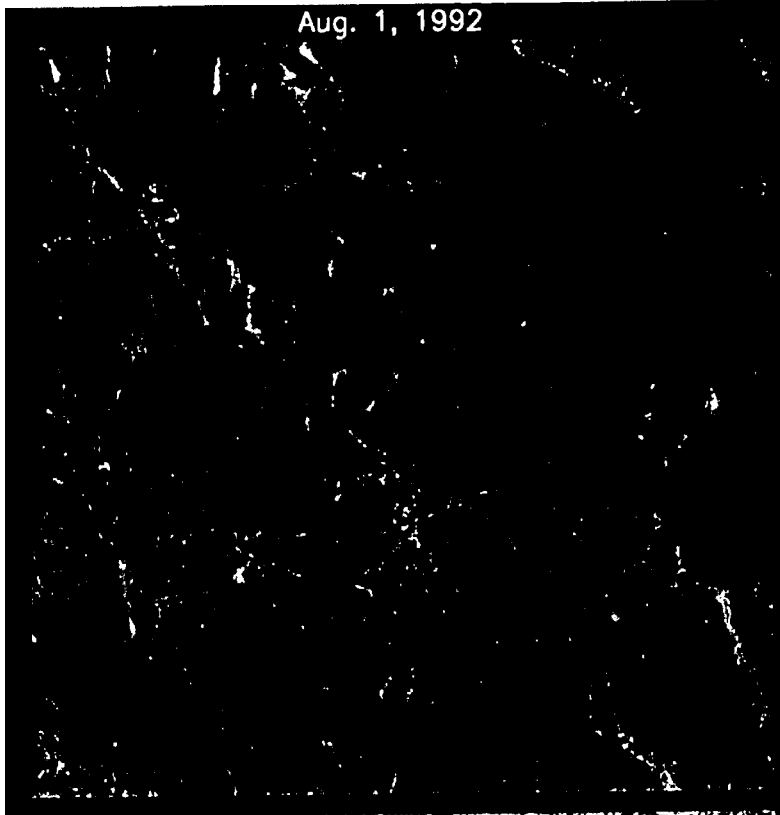




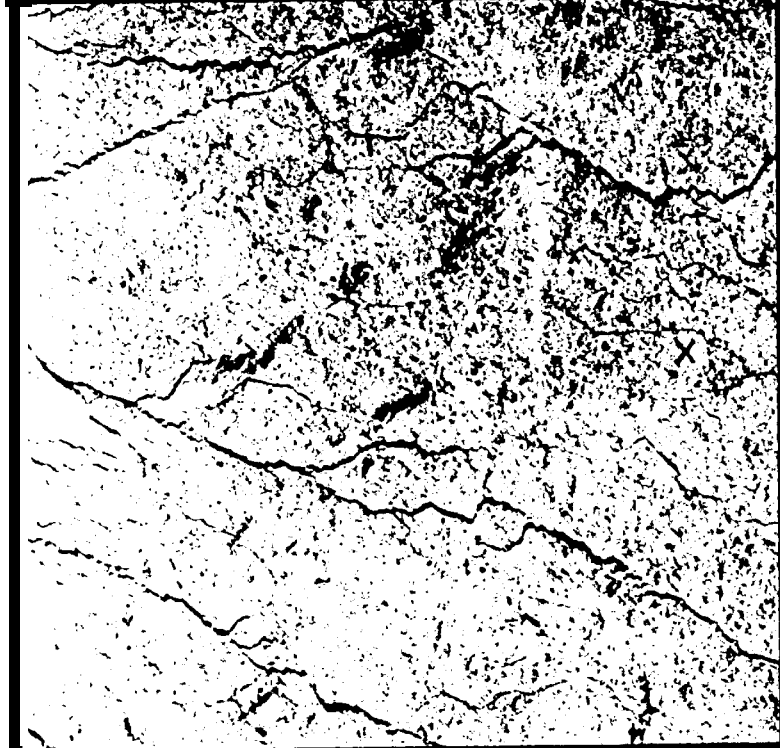
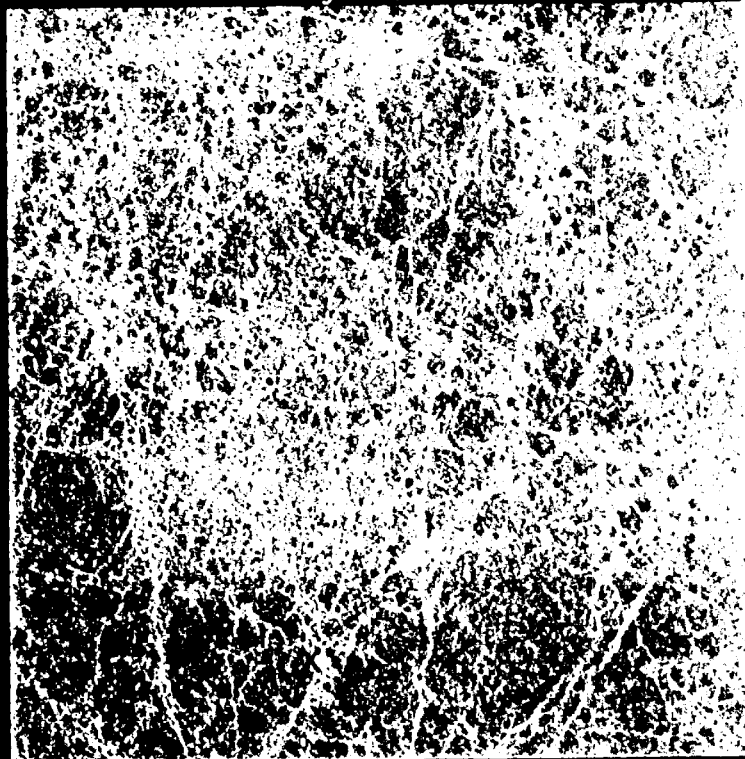


75° N

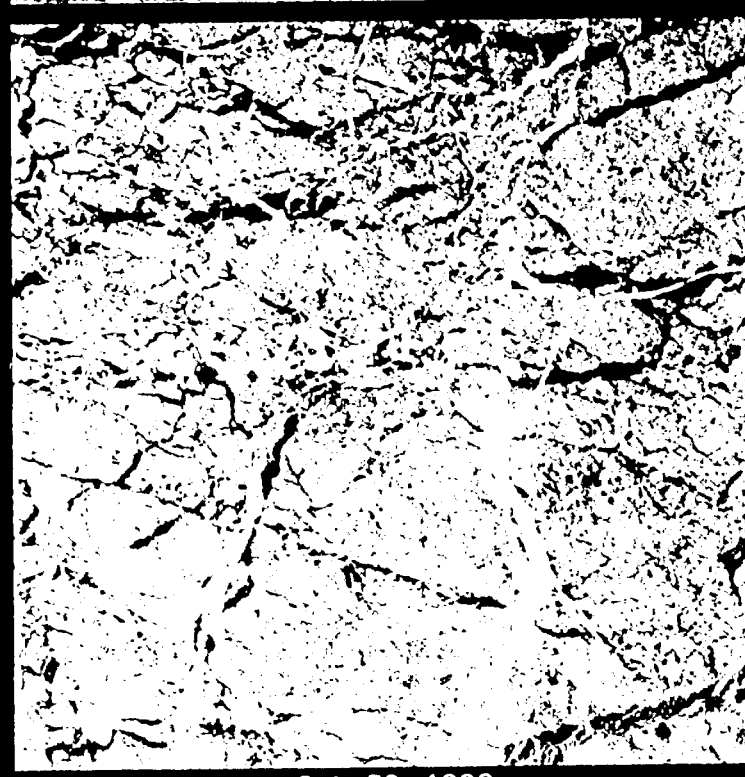
Aug. 1, 1992



Aug. 30, 1992



Sep. 28, 1992



Oct. 30, 1992

